Fast Exact Image Method for the Sommerfeld Half Space Problem

Jessica Piper
Center for Advanced Computation and Telecommunication
Department of Electrical and Computer Engineering
University of Massachusetts
Lowell, MA 01854 *

May 10, 2010

Abstract

The electric and magnetic fields due to a vertical electric dipole radiating over a half space of arbitrary permittivity and permeability are investigated. We model the dipole as an isotropic point source, and we use an exact image method to derive expressions for the reflected and transmitted fields. Our approach is similar to recent methods employing the Laplace Transform of the reflection coefficient. However, we calculate the Inverse Laplace Transform of the coefficient numerically, which allows us to simplify the remaining integral with a Hankel Transform. The resulting expression for the field converges quickly. Furthermore, we develop a numerical algorithm for calculating the field throughout the region, and verify our algorithm against direct evaluation of the Sommerfeld integrals.

*Jessica Piper was supported by NSF-REU grant No. CCF-0649235.

Contents

List of Figures

1 Overview and History of the Dipole Half-space Problem

The problem of a dipole radiator over a conducting half space has a long and contentious history. Early radio experimenters struggled to explain radio communications over distances greater than the line of site. In 1907, Zenneck published a solution for the electromagnetic potential which indicated the presence of a wave that travelled along the surface of the earth ("surface wave"). In 1909, Arnold Sommerfeld[1] published his own solution to the problem, which also presented evidence of the surface wave.

By the 1920's, researchers had realized that reflection from the ionosphere was the true enabler of long-distance radio transmission. However, the debate around Sommerfeld and Zenneck's earlier work had just begun. While Sommerfeld's 1909 solution supported the existence of surface waves, this paper is widely believed to contain a sign error. Sommerfeld's 1926 paper[2] corrected the sign error, but still the debate continued. Wait, in one of his final papers[3], gives a detailed history of the problem, its claims, and counter-claims. More recently, Collin has published an overview denying the sign error ever existed[4].

In addition to the sign or branch cut ambiguity, the Sommerfeld integrals had a bigger problem: the integrands were highly oscillatory and slow to converge. In the absence of digital computers, there was no fast numerical method for evaluating these types of integrals. Therefore, various alternative formulations of the integrals were proposed, including asymptotic expansions and alternate integration paths in the complex plane. Baños[5] gives a thorough overview of the state of this work up until the mid-1960's. The focus on transformed integration paths in the presences of poles and branch cuts has certainly exacerbated the problems related to the sign error.

Much of the historical work on the problem involved transforming the integrals into alternate formulations that were easy to compute. Modern computer power has largely obsoleted these efforts. In addition, computational Electromagnetics techniques such as Finite Difference Time Domain have greatly advanced in the last twenty years. Therefore, one may question why we might want a faster method to evaluate the Sommerfeld formulations. However, there are physical situations where techniques like FDTD and finite elements struggle: for example, very large or unbounded regions. Furthermore, the Sommerfeld formulations still have applications in areas like remote sensing.

In the 1980's, Lindell and Alanen published a series of three papers[6][7][8] where they employed an alternative approach to evaluating the integral. By using the Laplace-Transformed reflection coefficient, they obtained what they described as an exact image solution. However, their integral for the transformed reflection coefficient does not converge properly, and has to be approximated as a Taylor series. They obtained their expression for the Inverse Laplace Transform of the reflection coefficient by table look-up. However, their formulation of the reflection coefficient introduces a pole which does not in fact exist.

In the present work, we employ a method similar to Lindell and Alanen, but with a twist. We calculate the Inverse Laplace Transforms of the reflection and transmission coefficients directly. This allows us to use a Hankel Transform to simplify Sommerfeld's integral. Our method has the benefit that the transformed reflection (or transmission) coefficient only has to be numerically evaluated once, for an entire region. Then the field everywhere in the region can be calculated through a single integral, with the assistance of table look-up. Thus, our method offers a great computational advantage when examining the field over a large region.

The paper is structured as follows.

In Chapter 2 we derive the Sommerfeld Integrals for incident, reflected, and transmitted potential, starting with a 2-d Green's Function for the incident potential. In addition, we discuss numeric considerations in the direct numerical evaluation of the Sommerfeld integrals, and formally verify the validity of the Sommerfeld formulations.

In Chapter 3 we first introduce our method in outline form. The we discuss in detail the proper treatment of the reflection coefficient in order to calculate its Inverse Laplace Transform. We analyze the possible poles of the reflection coefficient, and find that there are none. Finally, we treat the branch cut, and demonstrate the validity of our transformation.

In Chapter 4, we derive the exact image solution for the reflected field. We also discuss an automated procedure for determining appropriate limits of integration.

In Chapter 5, we discuss our results, and present further areas for inquiry.

Supplementary material is included in the Appendix, including an overview of our notation conventions in Section 6.1, derivation of the free-space wave equation from Maxwell's equations in Section 6.2, an overview of the four-dimensional Fourier Transform representation of propagating waves and derivation of the lossy-medium wave equation in Section 6.3, an overview of the Laplace Transform in Section 6.4, and details of our use of the Hankel Transform in Section 6.5.

2 Derivation and Evaluation of the Sommerfeld Integrals

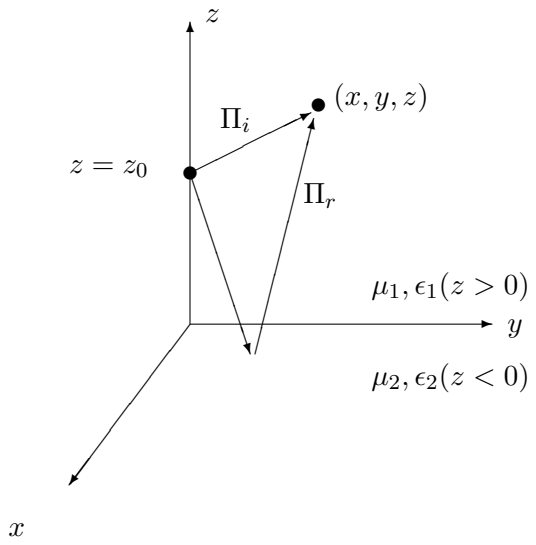

Figure 1: Point source over a half space

Consider a dipole located in the air, shown schematically in Fig 1. Below the dipole is the flat earth. If the dipole is small enough, we can consider it as a point source. This point source radiates isotropically. We'll assume the dipole is at $\vec{r_0} = (0, 0, z_0)$, and the boundary between the two media is the xy plane, $z = 0$.

We will assume that region 1, $z > 0$, is air, which we approximate by free space. The medium in region 2, $z < 0$, could be the ground, the ocean, the floor, or some other material. However, we will write our equations in such a way that the problem can be easily generalized later.

At an arbitrary point $\vec{r}$ in medium 1 ($z > 0$), the total field has contributions from direct radiation from the dipole, as well as radiation reflected from the material boundary. In medium 2 ($z < 0$), the total field is the transmitted field. We can find the reflected and transmitted potential by multiplying the incident field strength by the plane wave reflection and transmission coefficients respectively. Thus, our initial task is to find the potential function $\pi(\vec{r})$ that describes the incident field strength as a function of position.

Energy always radiates outward from a source, so the amplitude of $\pi(\vec{r})$ will be greatest at the source point, and then must decrease as we move away from the source in any direction. Therefore, the slope of the potential will be discontinuous at the source point.

We represent this discontinuity by a delta function, and then we derive a two-dimensional Green's Function, which matches the derivative of the potential to the discontinuity.

Our potential function must solve

$$\nabla^2\pi(\vec{r}) + k^2\pi(\vec{r}) = -\delta(x)\delta(y)\delta(z - z_0) \tag{1}$$

where $k = \omega\sqrt{\mu\epsilon}$ is the wavenumber, ω is the frequency of excitation, ϵ is the permittivity, μ is the permeability, $\pi(\vec{r})$ is the z-directed Hertz vector potential, and the delta functions represent the discontinuity at the source point. We will assume time-harmonic excitation with $e^{j\omega t}$ time dependence.

In the absence of the ground plane, a solution for our potential function is

$$\pi(\vec{r}) = \frac{Il}{4\pi j\epsilon\omega}\frac{e^{-jkR}}{R} \tag{2}$$

where I is the current density in the dipole, l is its length, and R is the distance between source and observation point. In the following sections, we use the normalization $Il/j\epsilon\omega = 1$ for clarity. However, the actual source term can be substituted in to the final equations.

The Sommerfeld solution uses a 2-d FT (Fourier Transform) instead of a 3-d FT due to the geometry of the problem. While the radiation emission is most easily described in spherical coordinates, the material boundary is a plane perpendicular to the z axis. Describing positions in reference to this plane is more convenient in cylindrical coordinates.

2.1 Two-dimensional Green's Function

We'll find $\pi(\vec{r})$ by first solving for $\Pi(\vec{\rho}, z)$, its two-dimensional Fourier Transform in the xy plane. That is,

$$\pi(\vec{r}) = \left(\frac{1}{2\pi}\right)^2 \int_{-\infty}^{\infty}\int_{-\infty}^{\infty} \Pi(\vec{\rho}, z)e^{-j\vec{\rho}\cdot\vec{r}}d\vec{k_x}d\vec{k_y} \tag{3}$$

where $\vec{\rho} = \vec{k_x} + \vec{k_y}$. For the rest of this section we'll omit the limits of integration for the benefit of brevity, but the limits remain $-\infty$ to $+\infty$ unless otherwise noted.

Remember that by definition:

$$\delta(x)\delta(y) = \left(\frac{1}{2\pi}\right)^2 \iint e^{-j(xk_x+yk_y)} d\vec{k_x} d\vec{k_y} = \left(\frac{1}{2\pi}\right)^2 \iint e^{-j\vec{\rho}\cdot\vec{r}} d\vec{k_x} d\vec{k_y} \tag{4}$$

Therefore, the FT of the right hand side of Eq (1) is:

$$-\delta(x)\delta(y)\delta(z-z_0) = -\left(\frac{1}{2\pi}\right)^2 \iint \delta(z-z_0) e^{-j\vec{\rho}\cdot\vec{r}} d\vec{k_x} d\vec{k_y} \tag{5}$$

The FT of $\nabla^2\pi(\vec{r})$ is:

$$\begin{aligned}
\nabla^2\pi(\vec{r}) &= \left(\frac{1}{2\pi}\right)^2 \iint \nabla^2\Pi(\vec{\rho},z) e^{-j\vec{\rho}\cdot\vec{r}} d\vec{k_x} d\vec{k_y} \\
&= \left(\frac{1}{2\pi}\right)^2 \iint \left((-k_x^2 - k_y^2)\Pi(\vec{\rho},z) + \frac{\partial^2}{\partial z^2}\Pi(\vec{\rho},z)\right) e^{-j\vec{\rho}\cdot\vec{r}} d\vec{k_x} d\vec{k_y} \\
&= \left(\frac{1}{2\pi}\right)^2 \iint \left(-\rho^2\Pi(\vec{\rho},z) + \frac{\partial^2}{\partial z^2}\Pi(\vec{\rho},z)\right) e^{-j\vec{\rho}\cdot\vec{r}} d\vec{k_x} d\vec{k_y}
\end{aligned}$$

Thus we can rewrite Eq (1) as:

$$\begin{aligned}
\left(\frac{1}{2\pi}\right)^2 \iint \left((k^2-\rho^2)\Pi(\vec{\rho},z) + \frac{\partial^2}{\partial z^2}\Pi(\vec{\rho},z)\right) e^{-j\vec{\rho}\cdot\vec{r}} d\vec{k_x} d\vec{k_y} = \\
-\left(\frac{1}{2\pi}\right)^2 \iint \delta(z-z_0) e^{-j\vec{\rho}\cdot\vec{r}} d\vec{k_x} d\vec{k_y}
\end{aligned} \tag{6}$$

But for this to be true, we require that:

$$\frac{\partial^2}{\partial z^2}\Pi(\vec{\rho},z) + (k^2-\rho^2)\Pi(\vec{\rho},z)) = -\delta(z-z_0) \tag{7}$$

First we'll solve for the complementary solution, where the right hand side is 0. We'll use Euler's solutions, keeping in mind that in our $e^{j\omega t}$ convention, e^{-jzk_z} represents travel in the positive z direction, while e^{jzk_z} represents travel in the negative z direction.

$$\Pi(\vec{\rho},z) = \begin{cases} Ae^{-jz\sqrt{k^2-\rho^2}}, & z > z_0 \\ Ce^{jz\sqrt{k^2-\rho^2}}, & z < z_0 \end{cases} \tag{8}$$

But $\Pi(\vec{\rho}, z)$ must be continuous at $z = z_0$, so

$$Ae^{-jz_0\sqrt{k^2-\rho^2}} = Ce^{jz_0\sqrt{k^2-\rho^2}} \tag{9}$$

We have two unknowns, so we need two equations. For our second equation, we'll integrate every term in Eq (7) with respect to z from z_0^- to z_0^+:

$$\int_{z_0^-}^{z_0^+} \frac{\partial^2}{\partial z^2}\Pi(\vec{\rho}, z)dz + (k^2 - \rho^2)\int_{z_0^-}^{z_0^+} \Pi(\vec{\rho}, z)dz = -\int_{z_0^-}^{z_0^+} \delta(z - z_0)dz \tag{10}$$

Remembering that $\Pi(\vec{\rho}, z)$ is continuous and that the integral of the delta function is 1 by definition, we can write:

$$\frac{\partial}{\partial z}\Pi(\vec{\rho}, z)|_{z_0^+} - \frac{\partial}{\partial z}\Pi(\vec{\rho}, z)|_{z_0^-} = -1 \tag{11}$$

Using the definitions for $\Pi(\vec{\rho}, z)$ from Eq (8), this becomes:

$$-j\sqrt{k^2-\rho^2}Ae^{-jz\sqrt{k^2-\rho^2}}|_{+z_0} - j\sqrt{k^2-\rho^2}Ce^{jz\sqrt{k^2-\rho^2}}|_{-z_0} = -1 \tag{12}$$

Solving for A in Eq (9) in terms of C, we can rewrite Eq (12) as:

$$j2\sqrt{k^2-\rho^2}Ce^{jz_0\sqrt{k^2-\rho^2}} = 1 \tag{13}$$

Solving for our constants, we can rewrite Eq (8), for all z, as:

$$\Pi(\vec{\rho}, z) = \frac{e^{-j|z-z_0|\sqrt{k^2-\rho^2}}}{j2\sqrt{k^2-\rho^2}} \tag{14}$$

Finally, we can express $\pi(\vec{r})$ as the IFT of $\Pi(\vec{\rho}, z)$:

$$\pi(\vec{r}) = \left(\frac{1}{2\pi}\right)^2 \int_{-\infty}^{\infty}\int_{-\infty}^{\infty} \frac{e^{-j|z-z_0|\sqrt{k^2-\rho^2}}}{j2\sqrt{k^2-\rho^2}} e^{-j\vec{\rho}\cdot\vec{r}}dk_x dk_y \tag{15}$$

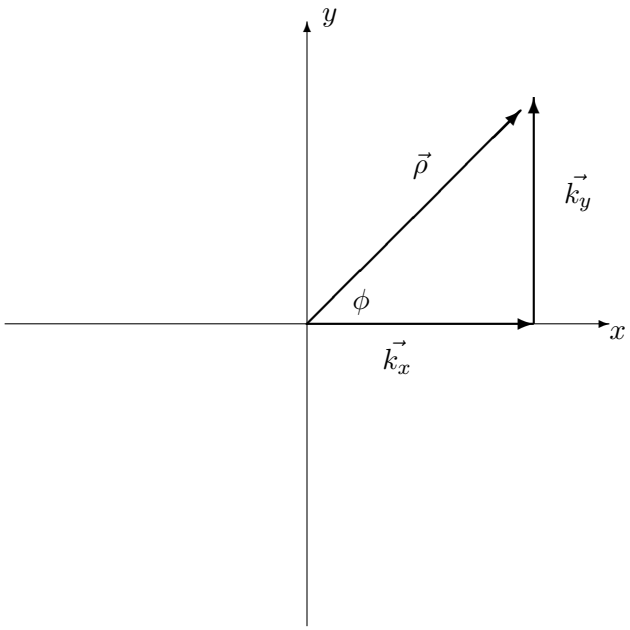

Figure 2: Orientation of wavenumber unit vectors in $k_x k_y$ plane

2.2 Translation of Green's Function to Cylindrical Coordinates

In the previous section, we used $\vec{\rho}$ as a shorthand for the Cartesian vector sum $\hat{x}k_x + \hat{y}k_y$. That is, ρ is the radial wavenumber magnitude in cylindrical coordinates. We will use ϕ as the angle in the $k_x k_y$ plane. See Fig 2. Likewise, we'll use γ and β as the magnitude and angle in the xy plane.

$$k_x k_y \text{ plane} \begin{cases} \vec{k_x} = \vec{\rho}\cos(\phi) \\ \vec{k_y} = \vec{\rho}\sin(\phi) \end{cases}$$

$$xy \text{ plane} \begin{cases} x = \vec{\gamma}\cos(\beta) \\ y = \vec{\gamma}\sin(\beta) \end{cases}$$

Using these definitions,

$$\vec{\rho} \cdot \vec{r} = \rho\gamma\cos(\phi - \beta) \tag{16}$$

A differential area in the $k_x k_y$ plane is $dk_x dk_y$. In cylindrical coordinates, a differential area is given by $\rho d\rho d\phi$. To cover the plane, we integrate ρ over $(0, \infty)$, and ϕ over $(0, 2\pi)$.

Thus, we can rewrite Eq (15) as:

$$\pi(\vec{r}) = \left(\frac{1}{2\pi}\right)^2 \int_0^{2\pi} \int_0^{\infty} \frac{e^{-j|z-z_0|\sqrt{k^2-\rho^2}}}{j2\sqrt{k^2-\rho^2}} e^{-j\rho\gamma\cos(\phi-\beta)} \rho d\rho d\phi \tag{17}$$

Integrating over ϕ, we get the Bessel Function $2\pi J_0(\rho\gamma)$. So we can write the field due to direct radiation from the source (the incident field) as:

$$\pi_i(\vec{r}) = \frac{1}{2\pi} \int_0^{\infty} \frac{e^{-j|z-z_0|\sqrt{k^2-\rho^2}}}{j2\sqrt{k^2-\rho^2}} J_0(\rho\gamma)\rho d\rho \tag{18}$$

Note that Eq (18) is in fact equal to Eq (2) – see eg[10]. This is sometimes called the Sommerfeld identity[11][12].

To obtain expressions for our reflected and transmitted wave potential, we multiply Eq (18) by the plane wave reflection and transmission coefficients, Γ and τ, and specify the sign of the $-j|z-z_0|$ term, according to the location of the image source and measurement point.

$$\pi_r(\vec{r}) = \frac{1}{2\pi} \int_0^{\infty} \frac{e^{-j(z+z_0)\sqrt{k^2-\rho^2}}}{j2\sqrt{k^2-\rho^2}} J_0(\rho\gamma)\Gamma(\theta_i, k_1, k_2)\rho d\rho \tag{19}$$

$$\pi_t(\vec{r}) = \frac{1}{2\pi} \int_0^{\infty} \frac{e^{j(z-z_0)\sqrt{k^2-\rho^2}}}{j2\sqrt{k^2-\rho^2}} J_0(\rho\gamma)\tau(\theta_i, k_1, k_2)\rho d\rho \tag{20}$$

Equations (18)-(20) are the Sommerfeld integrals for the incident, reflected, and transmitted fields respectively. Note that in the equation for the transmitted potential, the wavenumber and material properties corresponding to medium 2 should be used.

The reader familiar with the history of the Sommerfeld problem may note that Eq (19) is also commonly given in an alternate (though exact) formulation in terms of a Hankel function, where the limits of integration are from $-\infty$ to $+\infty$. The Hankel function formulation has an asymptotic representation, which is why it was commonly used in the past. In this paper, we only treat Eq (19), because it is of similar form to our ILT method, and because it is somewhat easier to evaluate exactly, because there is only one singularity along the integration path.

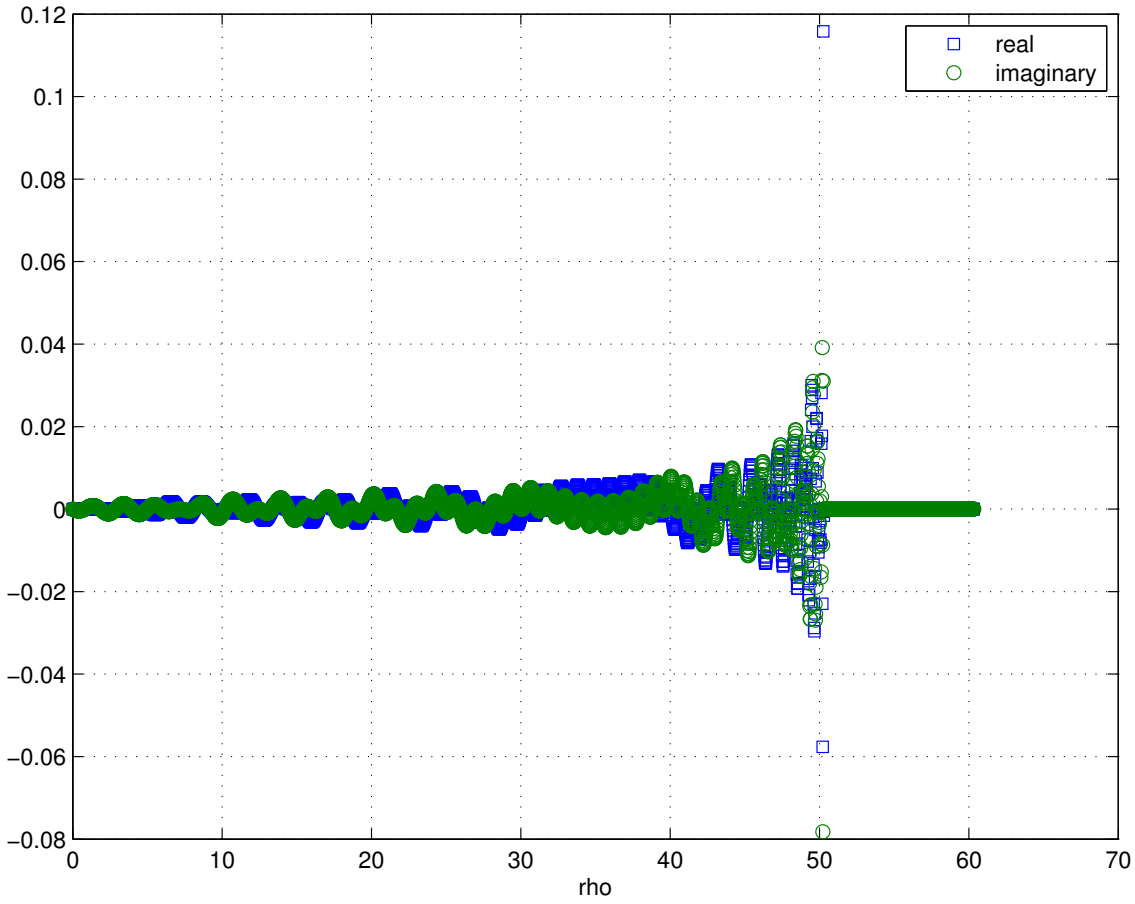

Figure 3: Sommerfeld Integrand - skipping singularity at $\rho = 50.26$

2.3 Numerical Evaluation of the Sommerfeld Integrals

The integrand (excluding reflection or transmission coefficient) for a Sommerfeld integral in shown in Fig 3. In this case, the frequency of the wave is 2.4 GHz, and the observation point is located 3 meters to the right and 3 meters above the source. These integrals provide several difficulties in evaluation: first, the singularity in the denominator must be handled properly, as well as the sign of the square root terms. Second, while the integral converges exponentially for $\rho > k$, the convergence for $\rho < k$ is slow. The Bessel function attenuates as $1/\sqrt{\rho}$, but due to the ρ term in the numerator, the integrand actually grows as $\sqrt{\rho}$. Furthermore, the oscillations of the exponential for $\rho < k$ can cause numerical difficulties. Finally, when the observation height is equal to the source height ($z = z_0$), the exponential term disappears, and the only convergence is due to the Bessel function and

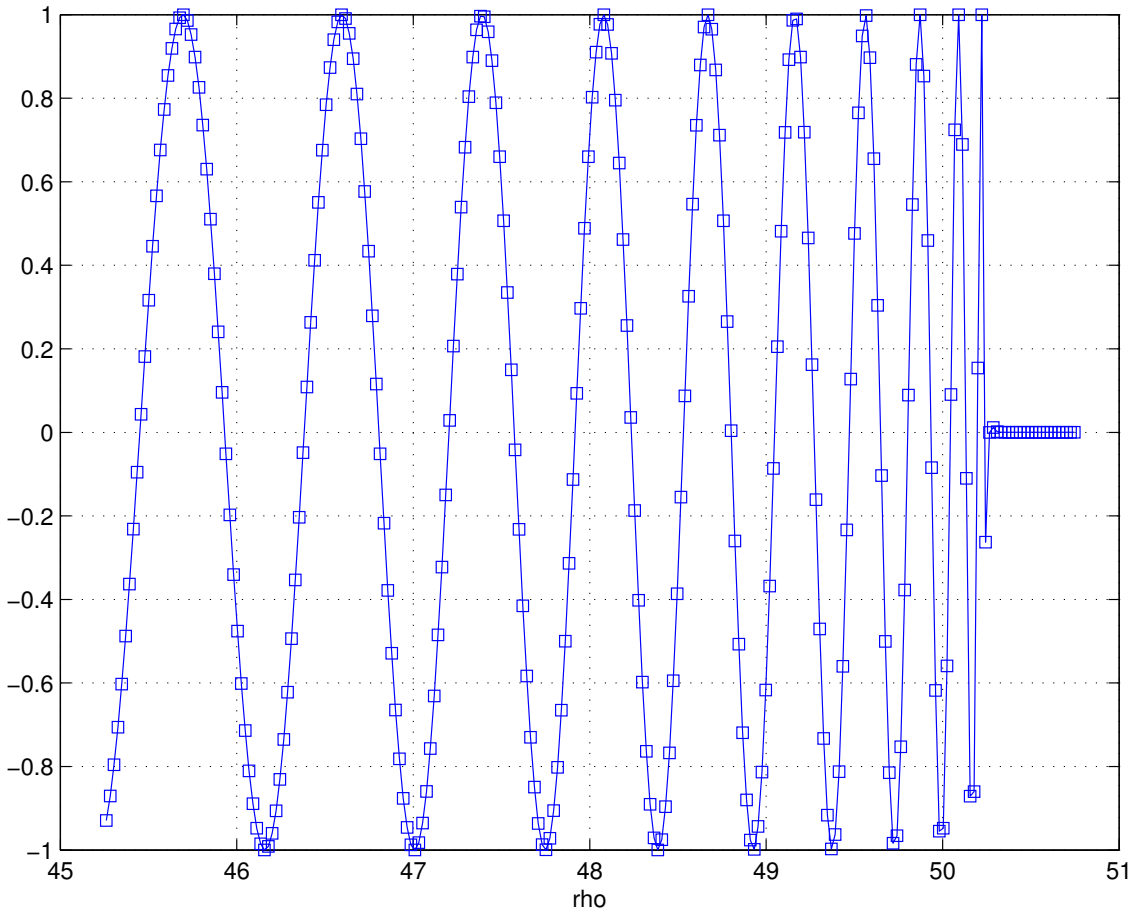

Figure 4: Real part of exponential as $\rho \to k$

the denominator.

As shown in Fig 4, as $\rho \to k$ the value of $\sqrt{k^2 - \rho^2}$ changes increasingly rapidly, and therefore the oscillations in the exponential are squeezed ever tightly together. If the numerical integration routine uses too large of a step size, the exponential term will provide a spurious contribution in the vicinity of $\rho = k$, due essentially to insufficient sampling. Using an adaptive integrator helps to mitigate this problem.

When $\rho > k$, we must choose that $\sqrt{k^2 - \rho^2} = -j\sqrt{\rho^2 - k^2}$ in order for the exponential to be bounded. For k real, this leaves us with only a real part, and so conversion of the integral becomes exponential.

The factor $\sqrt{k^2 - \rho^2}$ in the denominator is generally attenuating, except at $\rho = k$ where it

blows up. However, this singularity is integrable. Though the integrand becomes infinite, the contribution from this region is negligible. To see this, we split up the integral into four parts: a sum of two regions which avoid the singularity, and a sum of the regions just to either side of the singularity. The integrand is simply noted as I for clarity.

$$\pi_i(\vec{r}) = \frac{1}{2\pi} \cdot \lim_{\epsilon \to 0} \left(\int_0^{k-\epsilon} I d\rho + \int_{k+\epsilon}^{\infty} I d\rho \right) + \frac{1}{2\pi} \cdot \lim_{\epsilon \to 0} \left(\int_{k-\epsilon}^{k} I d\rho + \int_{k}^{k+\epsilon} I d\rho \right) \tag{21}$$

The first sum, which avoids the singularity, is finite for all $\epsilon > 0$. To show that the limit of the second sum is 0 as $\epsilon \to 0$, we will examine only the first term in detail, since the argument is the same for both terms.

For ϵ tiny, the exponential is approximately 1, and the Bessel is likewise essentially constant. Therefore:

$$\begin{aligned} &\lim_{\epsilon \to 0} \int_{k-\epsilon}^{k} \frac{e^{-j|z-z_0|\sqrt{k^2-\rho^2}}}{j2\sqrt{k^2-\rho^2}} J_0(\rho\gamma)\rho d\rho \\ &\quad \approx \lim_{\epsilon \to 0} \frac{J_0(k\gamma)}{4\pi j} \int_{k-\epsilon}^{k} \frac{\rho d\rho}{\sqrt{k^2-\rho^2}} \\ &\quad = \lim_{\epsilon \to 0} \frac{J_0(k\gamma)}{4\pi j} \left(-\sqrt{k^2-\rho^2} \right) |_{k-\epsilon}^{k} \approx 0 \end{aligned} \tag{22}$$

Because there is no contribution from the singularity, we can evaluate the incident Sommerfeld potential directly from:

$$\pi_i(\vec{r}) = \frac{1}{2\pi} \cdot \left(\int_0^{k-\epsilon} \frac{e^{-j|z-z_0|\sqrt{k^2-\rho^2}}}{j2\sqrt{k^2-\rho^2}} J_0(\rho\gamma)\rho d\rho + \int_{k+\epsilon}^{\infty} \frac{e^{-|z-z_0|\sqrt{\rho^2-k^2}}}{2\sqrt{\rho^2-k^2}} J_0(\rho\gamma)\rho d\rho \right) \tag{23}$$

with an appropriate choice for ϵ. For the results presented in this paper, MATLAB's adaptive Gaussian integrator `quadgk.m` was used, with $\epsilon = 10^{-9}$.

When $z = z_0$, the Sommerfeld integrand becomes

$$\pi_i(\gamma, z = z_0) = \frac{1}{2\pi} \int_0^{\infty} \frac{J_0(\rho\gamma)}{j2\sqrt{k^2-\rho^2}} \rho d\rho \tag{24}$$

The convergence of this integral is very slow, approximately $1/\sqrt{\rho}$. However, we can use Hankel Transforms to integrate this function exactly. The Hankel Transform is outlined in

the Bateman manuscript project, formerly titled *Tables of Integral Transforms*[15]. From Vol II, page 7, we can use Hankel Transforms #5 and #6 to obtain:

$$\pi_i(\gamma, z = z_0) = \frac{1}{4\pi\gamma}\left(\cos(k\gamma) - j\sin(k\gamma)\right) \tag{25}$$

(See Section 6.5 for details.) Therefore, in the special case of $z = z_0$, we can substitute the exact expression in Eq (25) for the integrand in Eq (19) and Eq (20) when evaluating the reflected and transmitted potentials.

2.4 Verification of Sommerfeld Identity

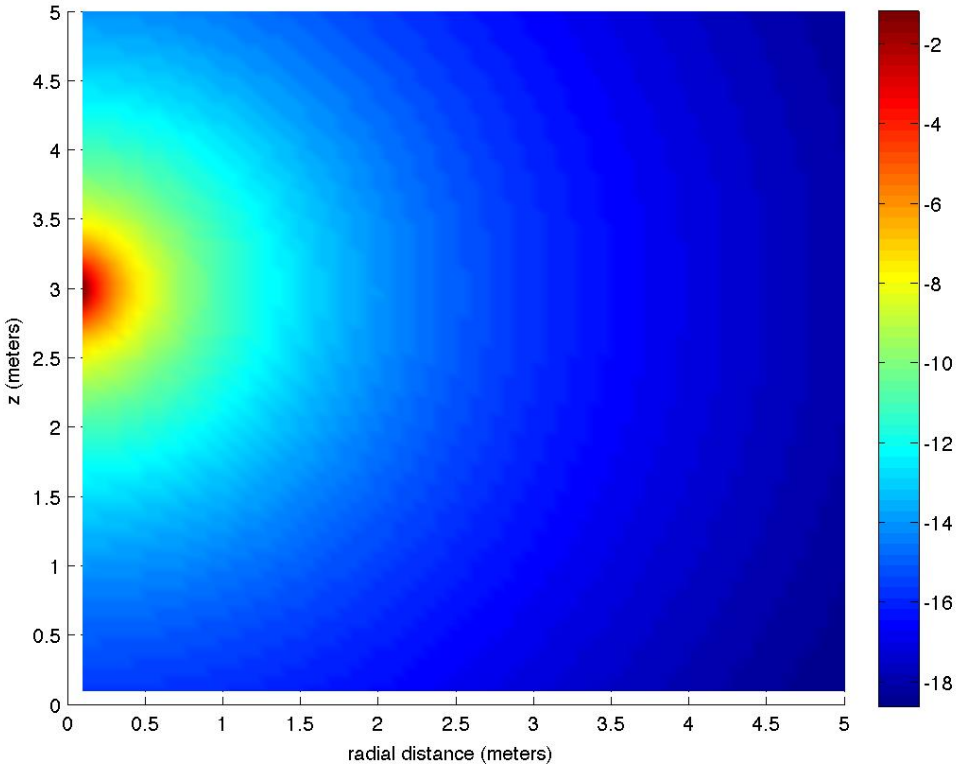

Figure 5: Incident power in free space, Sommerfeld formulation

Because the Sommerfeld integral for the incident potential, Eq (18), is an exact equivalent to the much simpler exponential representation in spherical coordinates, Eq (2), we can

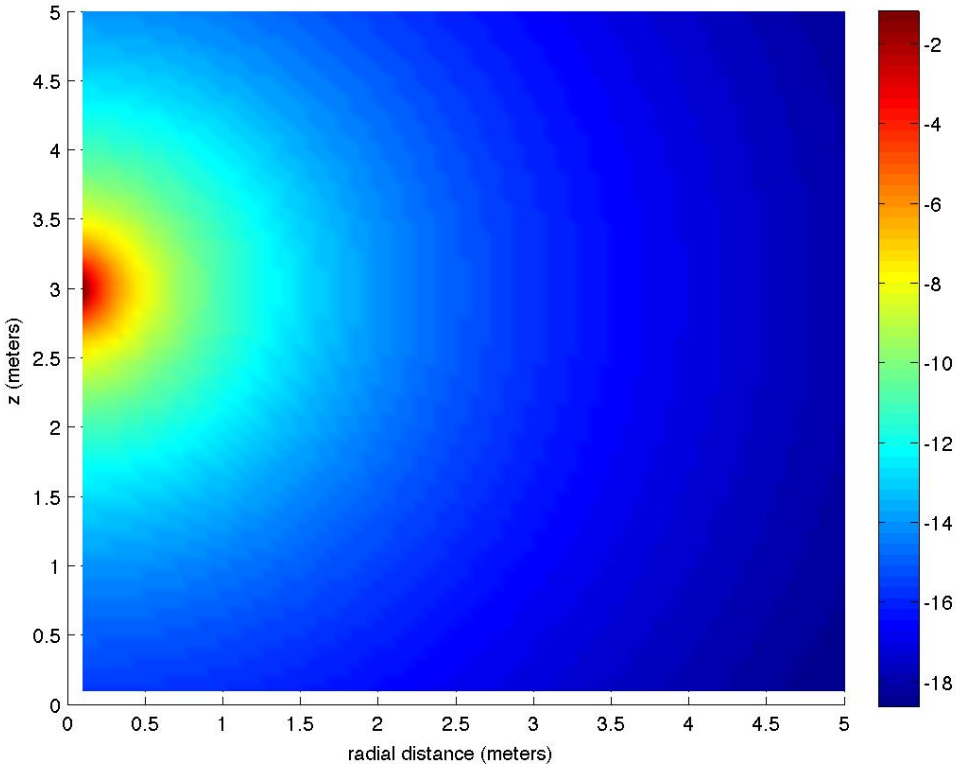

Figure 6: Incident power in free space, exponential formulation

validate our algorithm for evaluating the core of the Sommerfeld integral against the exact solution for the incident potential $\pi(\vec{r})$. The incident power for a dipole located at $z_0 = 3$ meters radiating in free space is shown using the Sommerfeld formulation in Fig 5, while the power calculated by the exponential formulation is shown in Fig 6. Obviously, the agreement is essentially exact.

To verify the Sommerfeld formulation for the reflected potential, we examine the reflected potential $\pi(\vec{r})$ as a function of the radial distance γ for a fixed observation height z. If we multiply the calculated potential by $4\pi R e^{jkR}$, where R is the distance from image source to observer, we counter the geometric attenuation, and therefore the potential will match the calculated reflection coefficient. In Fig 7 we plot the potential times the inverse of the geometric spreading ($\mathrm{pi_r}$), as well as the reflection coefficient (Gamma), as a function of angle, for the case of a 2.4 GHz signal reflected off of sea water. As can be seen, the potentials match exactly.

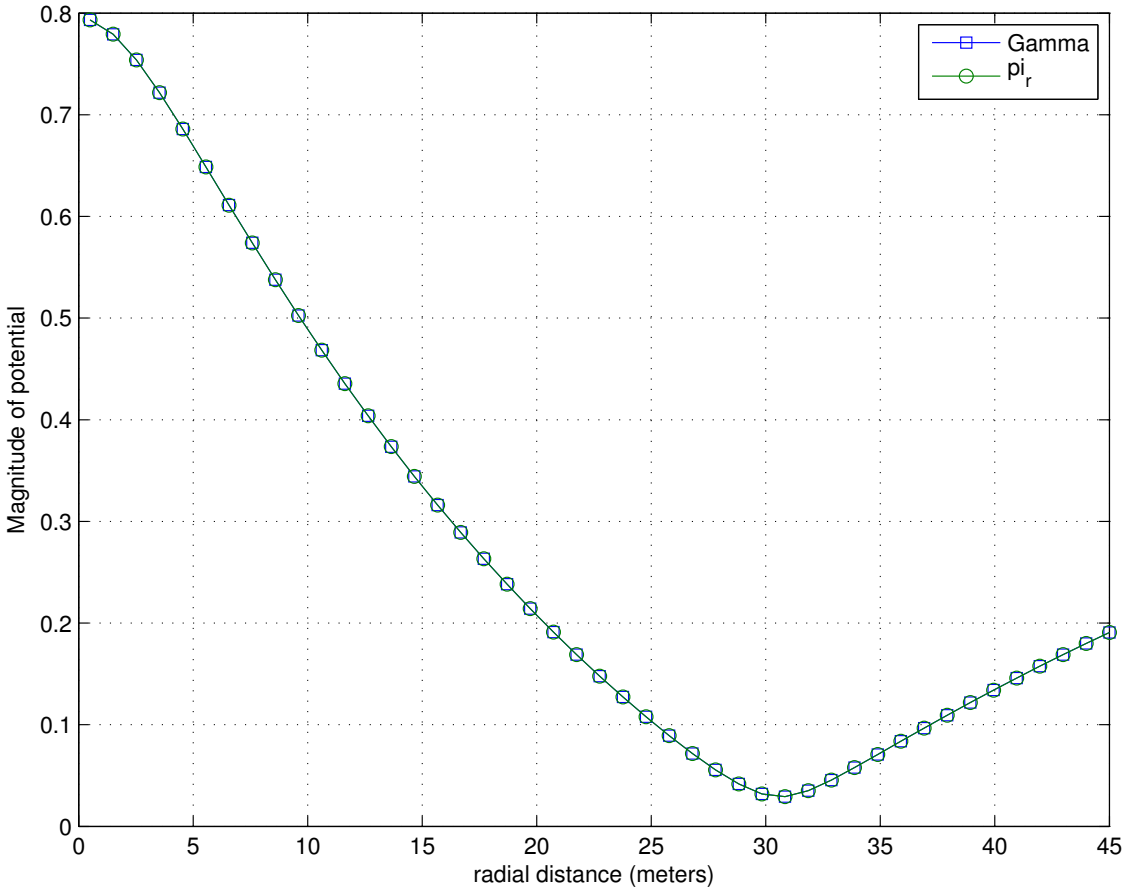

Figure 7: Potential reflected from sea water vs angle

3 Inverse Laplace Transform of Reflection coefficient

By replacing the reflection coefficient with its Inverse Laplace Transform (ILT), we are able to use a Hankel transform to simply the original Sommerfeld formulation for reflected potential. Likewise, we can use the same procedure to find the transmitted potential. We calculate the ILT of the coefficients numerically. Then to find the potential, we take the Laplace Transform (LT) of the transformed integrand times the ILT of the coefficient. Though the logic sounds circular, the results speak for themselves (see Section 5).

The following sections deal in depth with the treatment of the reflection and transmission coefficients. For details on the LT and ILT, see Section 6.4, in the Appendix.

3.1 Preparation of the reflection coefficient

For parallel polarization, the electric field vector $\vec{E}(\vec{r},t)$ lies in the plane of incidence. We will assume the magnetic field vector $\vec{H}(\vec{r},t)$ to be in the opposite direction for the incident and reflected waves. Then our plane wave reflection coefficient is given by:

$$\Gamma = \frac{\eta_2 \cos(\theta_t) - \eta_1 \cos(\theta_i)}{\eta_2 \cos(\theta_t) + \eta_1 \cos(\theta_i)} \tag{26}$$

Here θ_i is the angle of the incidence, θ_t is the angle of the transmission, and $\eta_i = \sqrt{\frac{\mu_i}{\epsilon_i}}$ is the impedance of the material. To accomplish our ILT, we want to re-formulate Γ in terms of θ_i, the magnitude of the incident wavenumber vector k_i and the material properties only.

Because there's no ϕ-dependence within the $k_x k_y$ plane, θ_i is the angle between $\vec{k_i}$ and the z-axis, as shown in Fig 8. So:

$$\sin(\theta_i) = \frac{\rho}{k_i} \tag{27}$$

Thus:

$$\cos(\theta_i) = \sqrt{1 - \left(\frac{\rho}{k_i}\right)^2} = \frac{\sqrt{{k_i}^2 - \rho^2}}{k_i} \tag{28}$$

From Snell's Law,

$$\sqrt{\mu_1 \epsilon_1}\sin(\theta_i) = \sqrt{\mu_2 \epsilon_2}\sin(\theta_t)$$

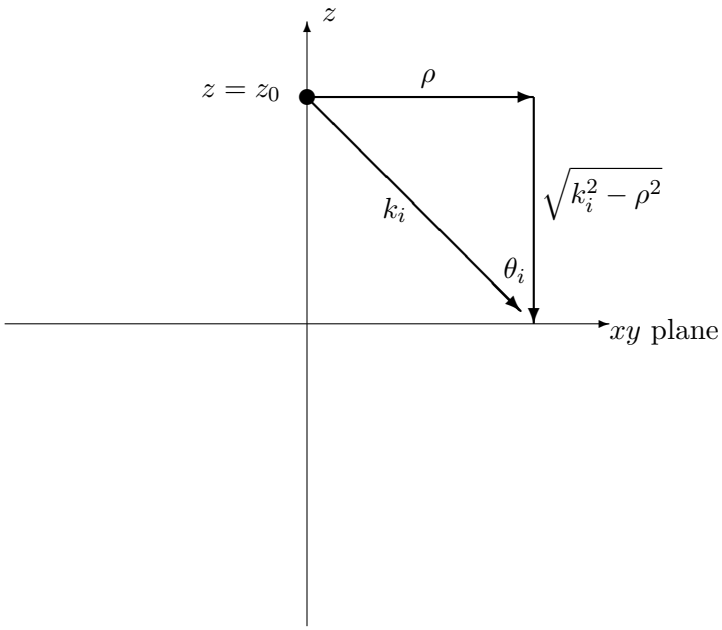

Figure 8: Decomposition of incident wave

and so

$$\cos^2(\theta_t) = 1 - \frac{1}{\mu\epsilon}\left(1 - \cos^2(\theta_i)\right) \tag{29}$$

where we define the normalized material properites:

$$\mu\epsilon = \frac{\mu_2\epsilon_2}{\mu_1\epsilon_1} \tag{30}$$

Then we can rewrite Eq (26) as:

$$\Gamma = \frac{\sqrt{\frac{\mu\epsilon - 1 + \cos^2\theta_i}{\mu\epsilon - 1}} - \epsilon\frac{\cos\theta_i}{\sqrt{\mu\epsilon - 1}}}{\sqrt{\frac{\mu\epsilon - 1 + \cos^2\theta_i}{\mu\epsilon - 1}} + \epsilon\frac{\cos\theta_i}{\sqrt{\mu\epsilon - 1}}} \tag{31}$$

or

$$\Gamma(q) = \frac{\sqrt{1 + q^2} - \epsilon q}{\sqrt{1 + q^2} + \epsilon q} \tag{32}$$

where

$$q = \frac{\sqrt{k_i^2 - \rho^2}}{k_i\sqrt{\mu\epsilon - 1}} = \frac{\cos\theta_i}{\sqrt{\mu\epsilon - 1}} \tag{33}$$

Our expression for $\Gamma(q)$ is not a proper rational fraction. In order to find its ILT, we need to rationalize it. First, we take the limit as $q \to \infty$, and subtract it from $\Gamma(q)$. This leaves us with the remainder, $R(q)$. That is,

$$\begin{aligned} \Gamma(q) &= \lim_{q\to\infty} \Gamma(q) + R(q) \\ &= \frac{1-\epsilon}{1+\epsilon} + R(q) \end{aligned} \tag{34}$$

With some algebraic manipulation, we can write:

$$R(q) = \frac{\epsilon}{1-\epsilon^2} \frac{\left(q - \sqrt{1+q^2}\right)^2 + \frac{1-\epsilon}{1+\epsilon}}{q^2 - \frac{1}{\epsilon^2-1}} \tag{35}$$

Next, we imagine that $\Gamma(q)$ is the LT of some unknown function $S(p)$. That is,

$$\Gamma(q) = \int_0^\infty S(p) e^{pq} dp \tag{36}$$

Therefore, by definition $S(p)$ is the ILT of $\Gamma(q)$. While previous authors have found $S(p)$ through table lookup [6][7], our method is to calculate $S(p)$ from the definition of the ILT:

$$S(p) = \frac{1}{j2\pi} \int_{-j\infty+\sigma}^{+j\infty+\sigma} \left(\frac{1-\epsilon}{1+\epsilon} + R(q)\right) e^{pq} dq \tag{37}$$

Here, q is still the normalization factor, while p is the Laplace Transform variable. That is, q retains the same physical meaning, but p has no physical meaning. We only use p to facilitate our calculations.

The constant term in the integrand of Eq (37) comes out along with a delta function in p. Then we can split off the integral of $R(q)$ for further analysis.

$$S(p) = \frac{1-\epsilon}{1+\epsilon}\delta(p) + \frac{1}{j2\pi}\int_{\sigma-j\infty}^{\sigma+j\infty} R(q)e^{pq}dq \tag{38}$$

$$= \frac{1-\epsilon}{1+\epsilon}\delta(p) + Ss(p) \tag{39}$$

The calculation of $Ss(p)$ is somewhat tricky. In general, q will be complex. So before we can evaluate $Ss(p)$, we need to examine $R(q)$ for poles, zeros, and branch points. There is a possible pole at $q = \pm\frac{1}{\sqrt{\epsilon^2-1}}$, and branch points at $q = \pm j$, from the term $\sqrt{1+q^2}$ in the numerator. Simply put, $\sqrt{1+q^2}$ is a multi-valued function, and therefore so is $R(q)$. We need to make sure we choose the correct value. Note that the possible poles are in fact the values of q corresponding to the Brewster Zero and the Zennek Pole. This issue is discussed in more depth in Section 5.5.

3.2 Analysis of Possible Poles

To analyze the possible poles, we expand the the numerator of Eq (35) in a Taylor Series at $a = \pm\frac{1}{\sqrt{\epsilon^2-1}}$, and examine the series as $q \to a$.

$$\begin{aligned} N(q) &= \sum_{n=0}^{\infty} \frac{N^{(n)}(a)}{n!}(q-a)^n \\ &= N(a) + N'(a)(q-a) + \dots \\ &= \left(a - \sqrt{1+a^2}\right)^2 + \frac{1-\epsilon}{1+\epsilon} - 2\left(\frac{a^2}{\sqrt{1+a^2}} - 2a + \sqrt{1+a^2}\right)(q-a) + \dots \end{aligned} \tag{40}$$

First, let's look at the case for $a = +\frac{1}{\sqrt{\epsilon^2-1}}$. Equation (40) reduces to:

$$-2\frac{(\epsilon-1)^2}{\epsilon\sqrt{\epsilon^2-1}}\left(q - \frac{1}{\sqrt{\epsilon^2-1}}\right) + F(a)\left(q - \frac{1}{\sqrt{\epsilon^2-1}}\right)^2 + \dots \tag{41}$$

The term $\left(q - \frac{1}{\sqrt{\epsilon^2-1}}\right)$ cancels the identical term in the denominator, so there is no pole in this case.

Next we examine $a = -\frac{1}{\sqrt{\epsilon^2-1}}$. We will choose $\sqrt{1+a^2} = -\frac{\epsilon}{\epsilon^2-1}$. So equation (40) reduces to:

$$2\frac{(\epsilon-1)^2}{\epsilon\sqrt{\epsilon^2-1}}\left(q+\frac{1}{\sqrt{\epsilon^2-1}}\right)+F(a)\left(q+\frac{1}{\sqrt{\epsilon^2-1}}\right)^2+\ldots \tag{42}$$

Here again, the term $\left(q+\frac{1}{\sqrt{\epsilon^2-1}}\right)$ cancels the identical term in the denominator. Thus, $R(q)$ is analytic everywhere in the complex plane. Therefore, the only contribution to the integral is from the branch points, which come from the $\sqrt{1+q^2}$ term.

3.3 Treatment of the branch cut

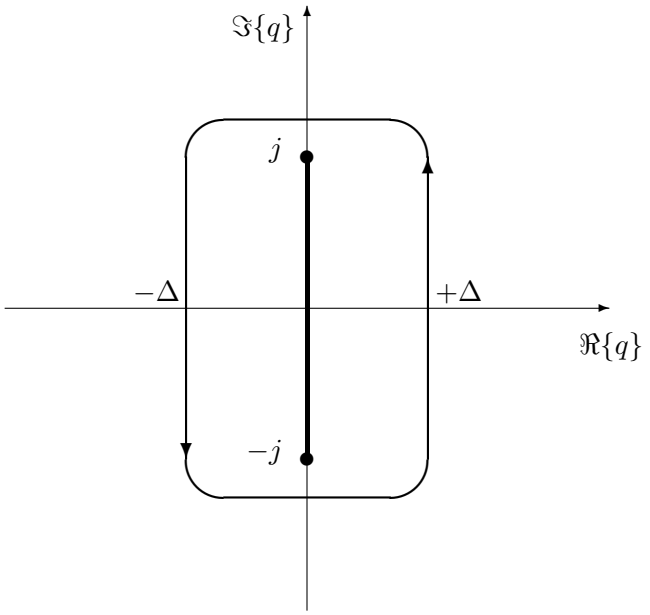

Figure 9: Contour for branch integral

We can carve out the source of the branch points, and call it $F(q)$:

$$F(q)=\frac{\epsilon}{\epsilon^2-1}\frac{2q\sqrt{1+q^2}}{q^2-\frac{1}{\epsilon^2-1}} \tag{43}$$

As defined in Eq (95) in Sec 6.4, the ILT is a line integral in the complex plane over $(\sigma-j\infty,\sigma+j\infty)$. For the integral to converge, we choose σ to be to the right of any singularities. In the present case, we have no singularities, so we don't have to worry about them. In addition, we already know that $F(q)\to 0$ as $q\to\infty$, because $R(q)$ (and therefore $F(q)$ as well) is a proper, rational fraction.

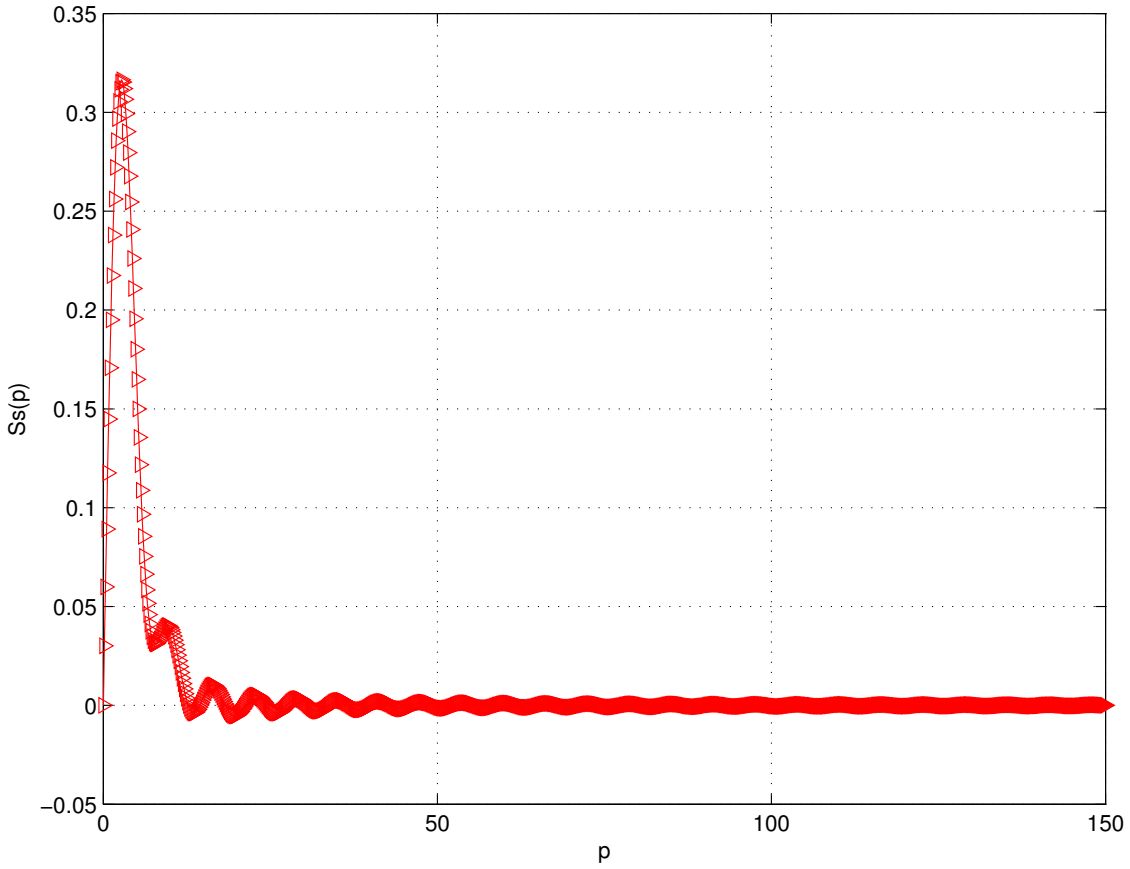

Figure 10: ILT of R(q), $\epsilon = 3 - .1i$

Because the value of the integral is zero everywhere except at the branch points, we can draw an equivalent contour closely encircling the two branch points. See Fig 9. We will treat this integral as the sum of two line integrals, on either side of the imaginary axis, between $z = \pm j$. For $+\Delta$ we choose $+\sqrt{1+q^2}$, and for $-\Delta$, we choose $-\sqrt{1+q^2}$. But we will evaluate the integral in the limit as $\Delta \to 0$.

$$Ss(p) = \lim_{\Delta \to 0} \frac{1}{j2\pi} \left(\int_{-j+\Delta}^{+j+\Delta} F(q) e^{pq} dq + \int_{+j-\Delta}^{-j-\Delta} F(q) e^{pq} dq \right) \tag{44}$$

Using the substitution $q = jy$, we can transform this integral into the following form, ideally suited to numerical integration:

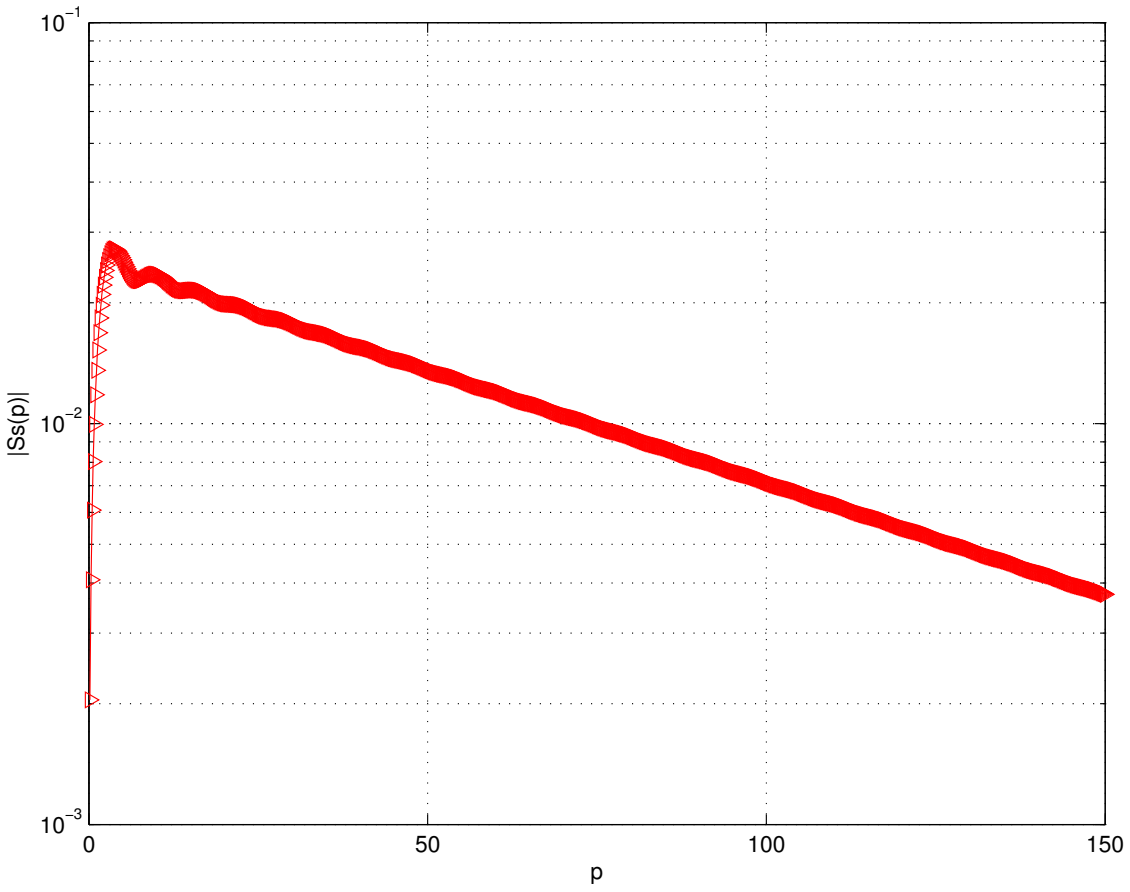

Figure 11: ILT of R(q), $\epsilon = 76 - 10i$

$$Ss(p) = \frac{4\epsilon}{\pi} \int_0^1 \frac{y\sqrt{1-y^2}}{(\epsilon^2-1)y^2+1} \sin(py)dy \tag{45}$$

Figure 10 shows the real part of $Ss(p)$ for $\epsilon = 3 - .1i$, corresponding to dry sand. As can be seen, the magnitude of $Ss(p)$ quickly drops to nearly 0, but then continues to oscillate with a very slowly decreasing amplitude. In contrast, Fig 11 shows $Ss(p)$ for $\epsilon = 76 - 10i$, corresponding to sea water. Here the straight descent on the logarithmic y axis shows exponential decrease.

To ensure that the branches were handled correctly in the foregoing analysis, $\hat{\Gamma}(q)$ was calculated from Eq (36), and plotted along with $\Gamma(q)$ versus θ_i. At the top of each plot, the upper limit of integration for p is listed. Figure 12 shows the case for $\epsilon = 3$. The upper

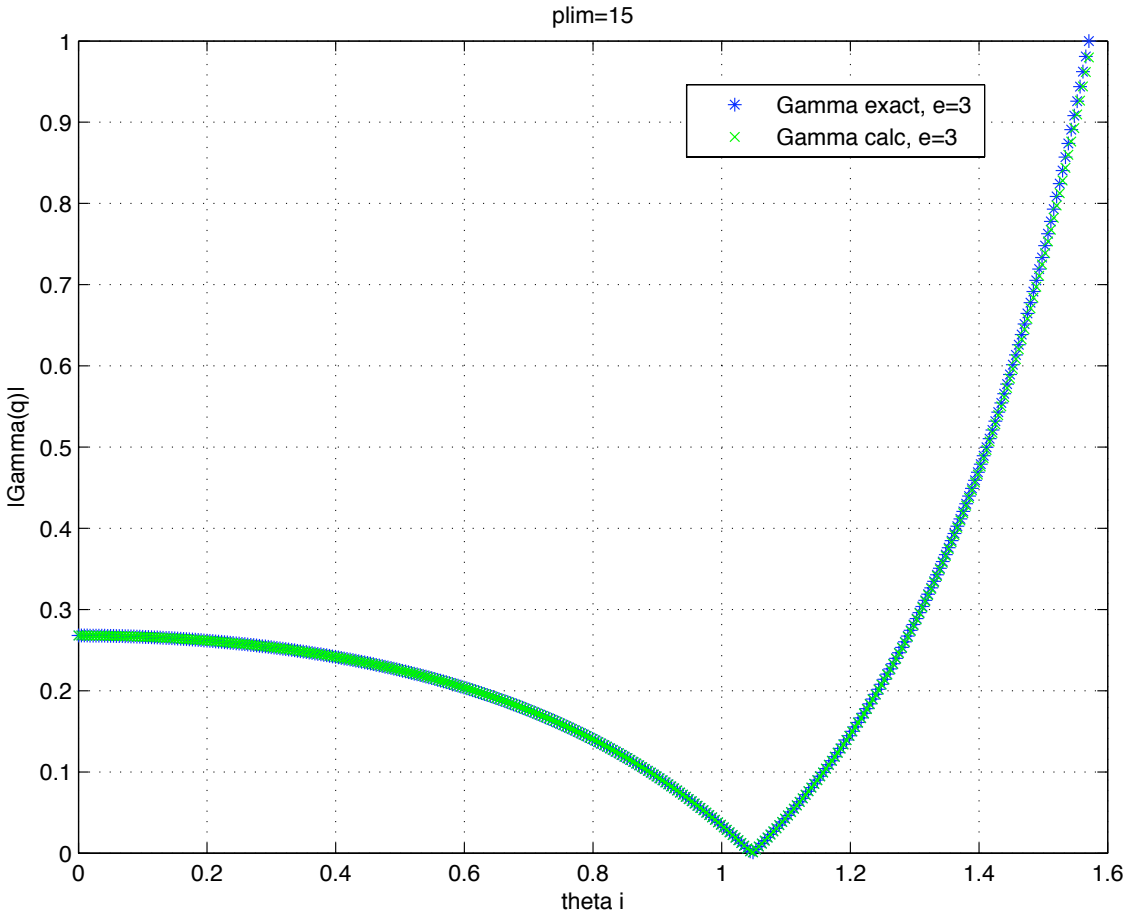

Figure 12: $\Gamma(q)$ vs ILT of LT of $\Gamma(q)$

limit of integration for p in this case was only 15. Figure 13 shows the case for $\epsilon = 80$. The upper limit of integration was raised to 200 to get good agreement.

In Figure 14, we see the case for a leaky dielectric with $\epsilon = 10 - 10i$. Here the upper limit of p was 70. Finally, in Figure 15 we see the case of a conductive plasma. In this case, $p \to 450$ was not enough for close agreement as $\theta_i \to \pi/2$. In general, as the incidence approaches grazing, the computation becomes more difficult.

In conclusion, we can use the following formula to calculate $S(p)$:

$$S(p) = \frac{1-\epsilon}{1+\epsilon}\delta(p) + \frac{4\epsilon}{\pi}\int_0^1 \frac{y\sqrt{1-y^2}}{(\epsilon^2-1)y^2+1}\sin(py)dy \tag{46}$$

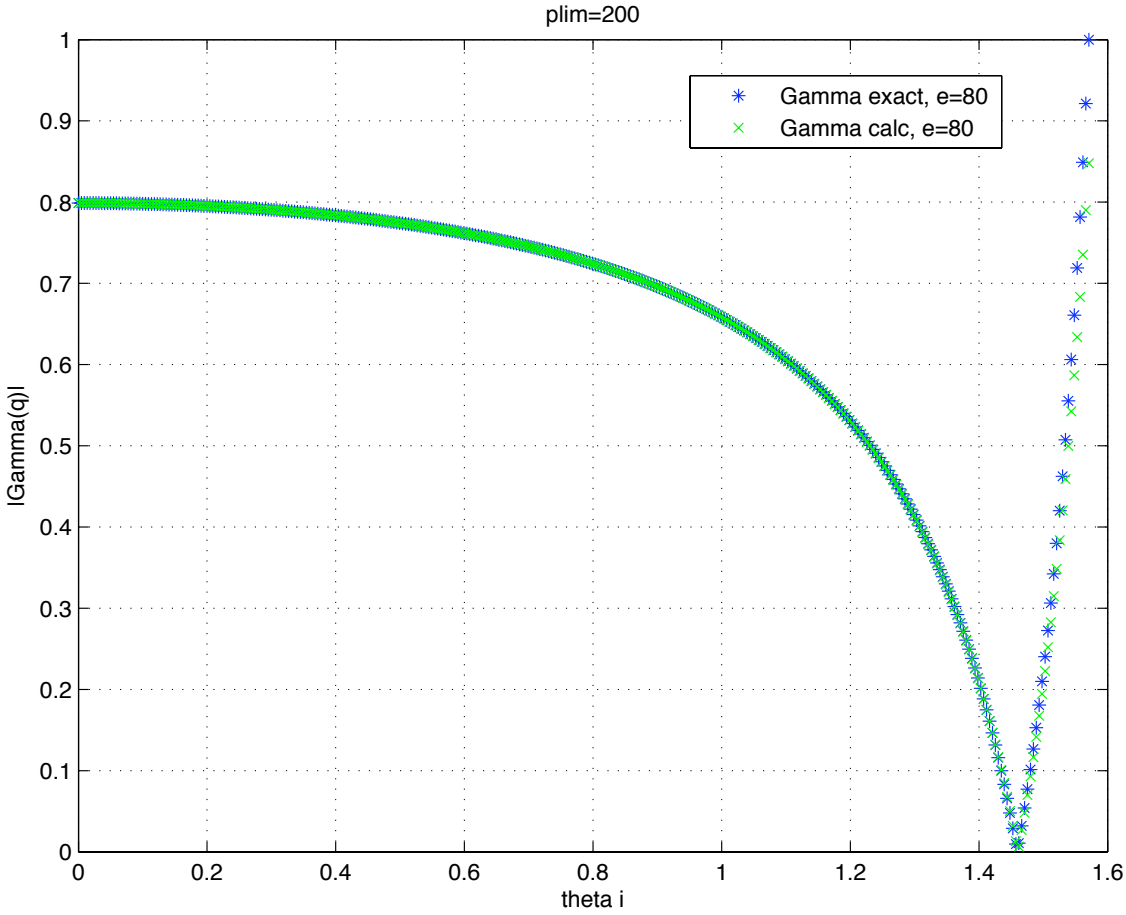

Figure 13: $\Gamma(q)$ vs ILT of LT of $\Gamma(q)$

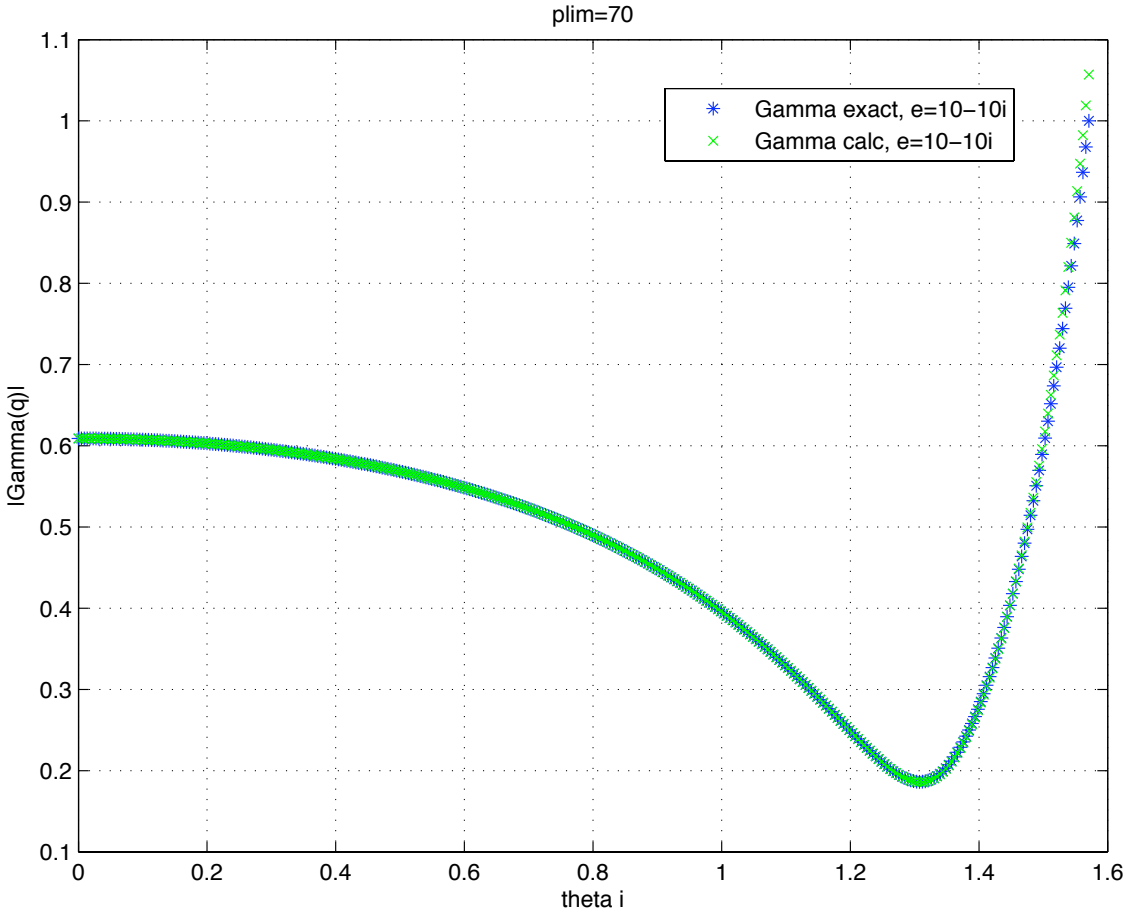

Figure 14: $\Gamma(q)$ vs ILT of LT of $\Gamma(q)$

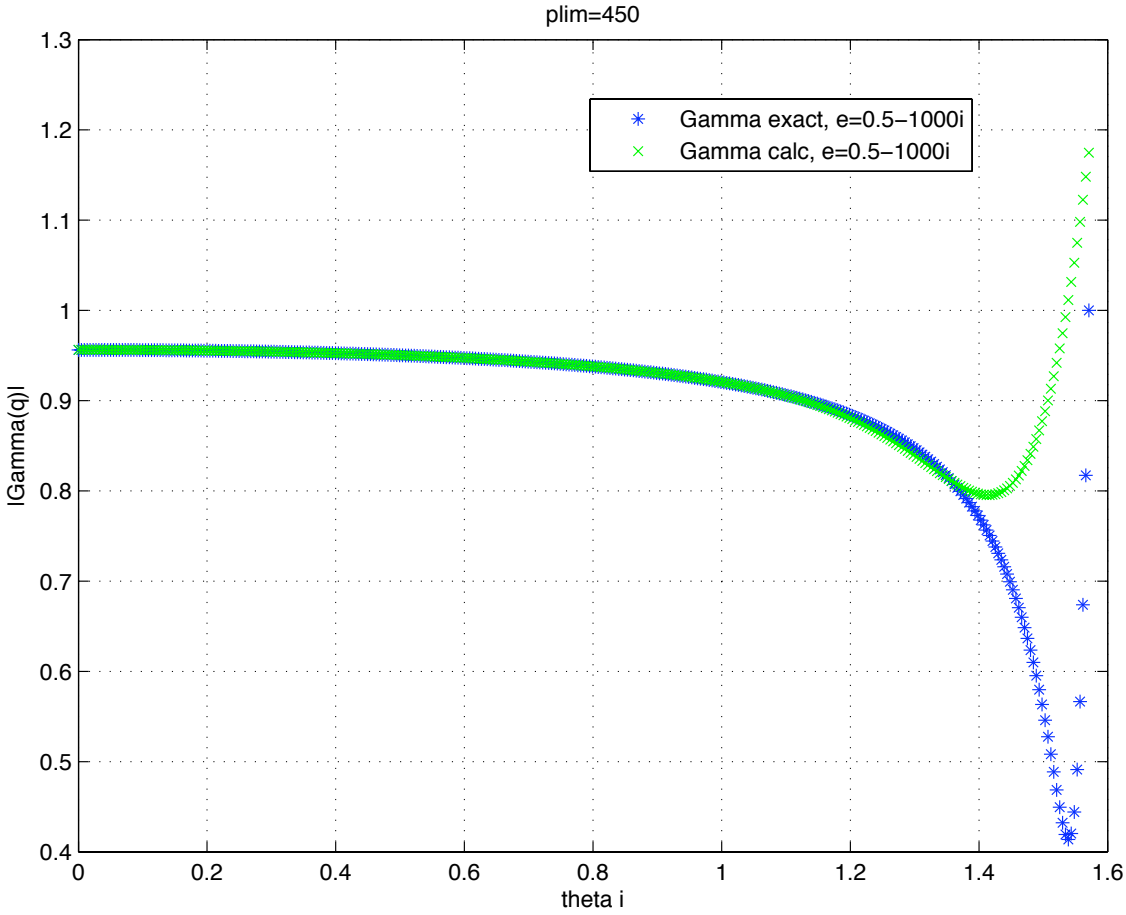

Figure 15: $\Gamma(q)$ vs ILT of LT of $\Gamma(q)$

4 Exact Image Solution for Reflected Field

Using the tools previously developed, we can now find expressions for the total potential due to the reflected and transmitted waves.

4.1 Detailed derivation for Reflected Field

Using Eq (19) from page 11 and Eq (46), we can write our formula for the reflected field as:

$$\pi_r(\vec{r}) = \frac{1}{2\pi}\int_0^\infty \frac{e^{-j(z+z_0)\sqrt{k^2-\rho^2}}}{j2\sqrt{k^2-\rho^2}} J_0(\rho\gamma)\int_0^\infty S(p)e^{pq}dp\rho d\rho \tag{47}$$

By changing the order of integration and replacing q by its definition we get:

$$\pi_r(\vec{r}) = \frac{1}{2\pi}\int_0^\infty S(p)\int_0^\infty \frac{e^{-j(z+z_0)\sqrt{k^2-\rho^2}}}{j2\sqrt{k^2-\rho^2}} J_0(\rho\gamma)e^{p\frac{\sqrt{k^2-\rho^2}}{k\sqrt{\mu\epsilon-1}}}\rho d\rho dp \tag{48}$$

Let $\alpha = z + z_0 - \frac{jp}{k\sqrt{\mu\epsilon-1}}$. Then we can rewrite Eq (48) as:

$$\pi_r(\vec{r}) = \frac{1}{2\pi}\int_0^\infty S(p)\int_0^\infty \frac{e^{-j\alpha\sqrt{k^2-\rho^2}}}{j2\sqrt{k^2-\rho^2}} J_0(\rho\gamma)\rho d\rho dp \tag{49}$$

Now we can apply the Hankel Transform (see section 6.5 for details), with the result:

$$\pi_r(\vec{r}) = \frac{1}{4\pi}\int_0^\infty S(p)\frac{e^{-jk\psi}}{\psi}dp \tag{50}$$

where $\psi = \sqrt{x^2+y^2+\left(z+z_0-\frac{jp}{k\sqrt{\mu\epsilon-1}}\right)^2}$. This can be thought of as a "complex distance," following the lead of Wait[14].

Referring to Fig 16, the total (physical) distance from the image source to the measurement point is

$$\zeta = \sqrt{x^2+y^2+(z+z_0)^2} \tag{51}$$

Therefore we can define

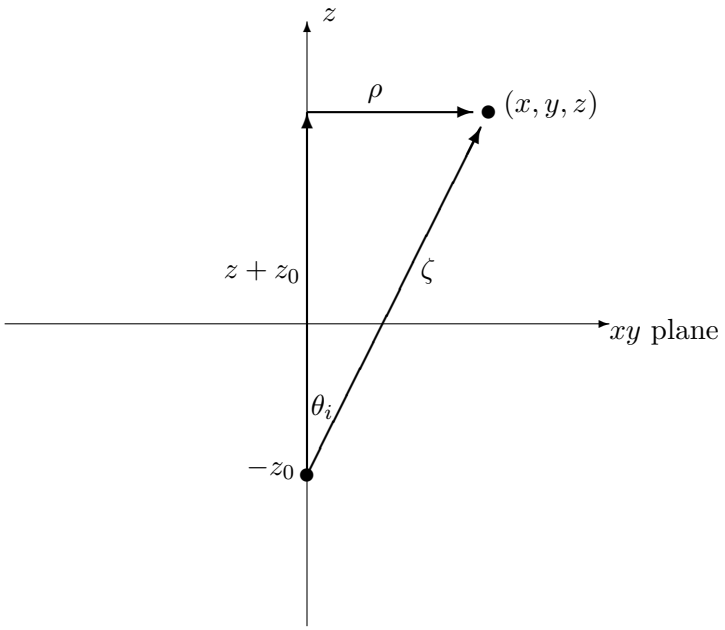

Figure 16: Reflected field due to image source

$$\xi = \frac{\psi}{\zeta} = \sqrt{1 - \left(\frac{p}{\zeta k\sqrt{\mu\epsilon - 1}}\right)^2 - j\frac{2p(z + z_0)}{\zeta^2 k\sqrt{\mu\epsilon - 1}}} \tag{52}$$

But referring again to Fig 16 we see that:

$$\frac{z + z_0}{\zeta} = \cos\theta_i \tag{53}$$

So we can write:

$$\xi = \sqrt{1 - \left(\frac{p}{\zeta k\sqrt{\mu\epsilon - 1}}\right)^2 - j\frac{2p\cos\theta_i}{\zeta k\sqrt{\mu\epsilon - 1}}} \tag{54}$$

Using the definition of $S(p)$ from Eq (39) in the equation for $\pi_r(\vec{r})$ (49) we get

$$\pi_r(\vec{r}) = \frac{1}{4\pi}\int_0^\infty \frac{1-\epsilon}{1+\epsilon}\delta(p)\frac{e^{-jk\psi}}{\psi}dp + \frac{1}{4\pi}\int_0^\infty Ss(p)\frac{e^{-jk\psi}}{\psi}dp \tag{55}$$

But notice, $\psi|_{p=0} = \zeta$. Thus:

$$\pi_r(\vec{r}) = \frac{e^{-jk\zeta}}{4\pi\zeta}\left(\frac{1-\epsilon}{1+\epsilon} + \int_0^\infty Ss(p)\frac{e^{-jk\zeta(\xi-1)}}{\xi}dp\right) \tag{56}$$

In Eq (56), the leading factor $\frac{e^{-jk\zeta}}{4\pi\zeta}$ represents spherical attenuation, just as in our initial free-space solution for incident potential. By definition, this geometric attenuation is absent in a plane wave. But for $\zeta \to \infty$, we should be able to use the plane wave approximation, discounting spherical attenuation. In other words,

$$\lim_{\zeta\to\infty}\left(\frac{4\pi\zeta}{e^{-jk\zeta}}\right)\pi_r(\vec{r}) = \Gamma(q) \tag{57}$$

By expressing ξ as its binomial expansion, we can prove this equivalence.

$$\xi = 1 - \frac{1}{2}\left(\frac{p}{\zeta k\sqrt{\mu\epsilon - 1}}\right)^2 - j\frac{p\cos\theta_i}{\zeta k\sqrt{\mu\epsilon-1}} + \ldots \tag{58}$$

Then

$$\lim_{\zeta\to\infty}\xi = 1 \qquad \text{and} \qquad \lim_{\zeta\to\infty} -jk\zeta\,(\xi-1) = \frac{-p\cos\theta_i}{\sqrt{\mu\epsilon-1}}$$

Therefore, taking the limit of Eq (56) we have:

$$\lim_{\zeta\to\infty}\pi_r(\vec{r}) = \frac{1-\epsilon}{1+\epsilon} + \int_0^\infty Ss(p)e^{-pq}dp = \Gamma(q) \tag{59}$$

Which is the desired result. To verify this procedure, the reflected potential was calculated as a function of angle of incidence for a source a fixed distance from the medium boundary. Then this potential was multiplied by $4\pi\zeta e^{jk\zeta}$ to cancel the spherical attenuation. In Figures 17 and Fig 18, we consider the reflected potential due to a 2.4 GHz wave incident from 2 meters onto dry sand, as a function of angle. In the graphs, Gamma is the reflection coefficient, and Pi is the calculated potential. As can be seen in Fig 17, the magnitude agreement is very good. However, in Fig 18, we see that the ILT method has introduced a spurious imaginary part.

In Fig 19, which plots the magnitude of the reflected field for a 2.4 GHz signal incident from 2 meters onto sea water, we see that the overall agreement is good except in the region of the Brewster zero, which corresponds to total transmission. These observations are discussed in more detail in Section 5.

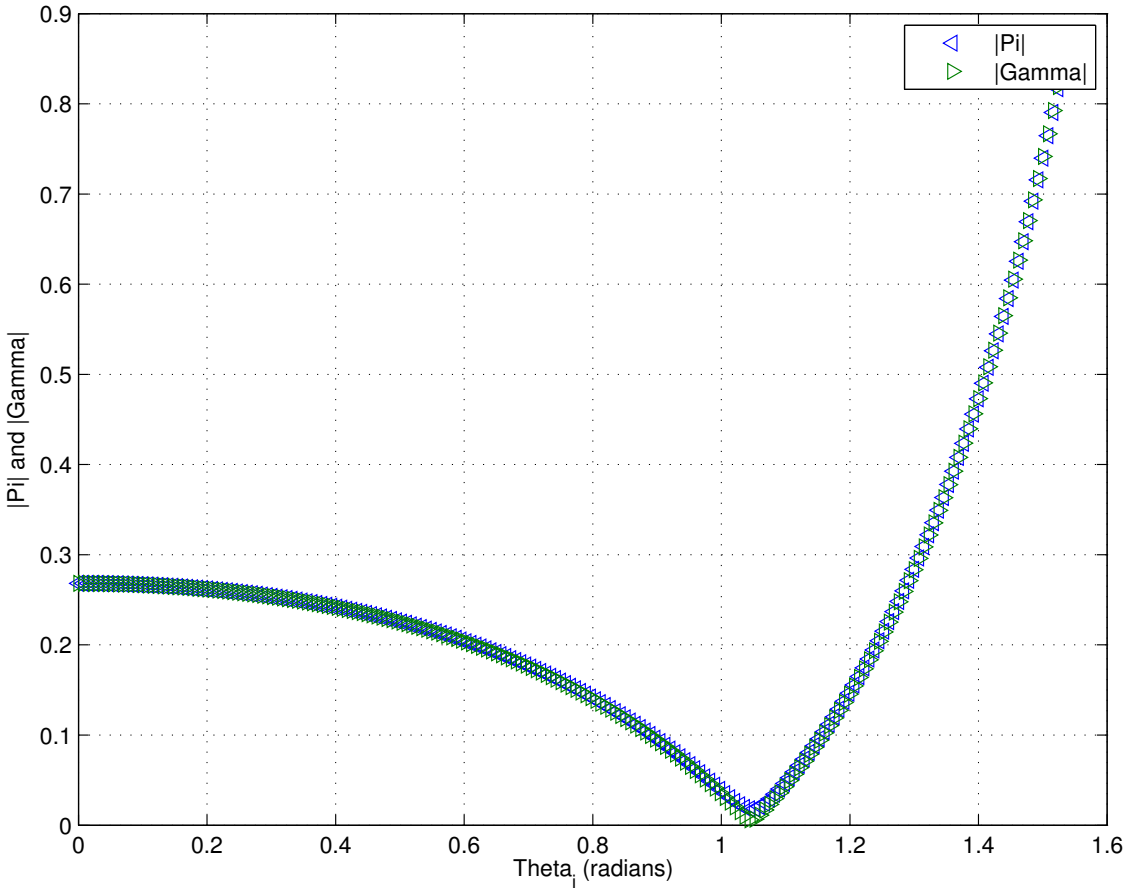

Figure 17: Verification of ILT method - magnitude of field reflected from sand

In conclusion, we can calculate the reflected field using the nested integral:

$$\pi_r(\vec{r}) = \frac{e^{-jk\zeta}}{4\pi\zeta}\left(\frac{1-\epsilon}{1+\epsilon} + \frac{4\epsilon}{\pi}\int_0^\infty \int_0^1 \frac{y\sqrt{1-y^2}}{(\epsilon^2-1)y^2+1}\sin(py)dy\frac{e^{-jk\zeta(\xi-1)}}{\xi}dp\right) \tag{60}$$

However, when calculating the field throughout a region, it is more convenient to determine the maximum value of p needed in a region, and then create a lookup table of values of $Ss(p)$ as a function of p. This speeds the calculation considerably. Details of this procedure, as well as an automated method to find the limits of integration, are given in 4.2.

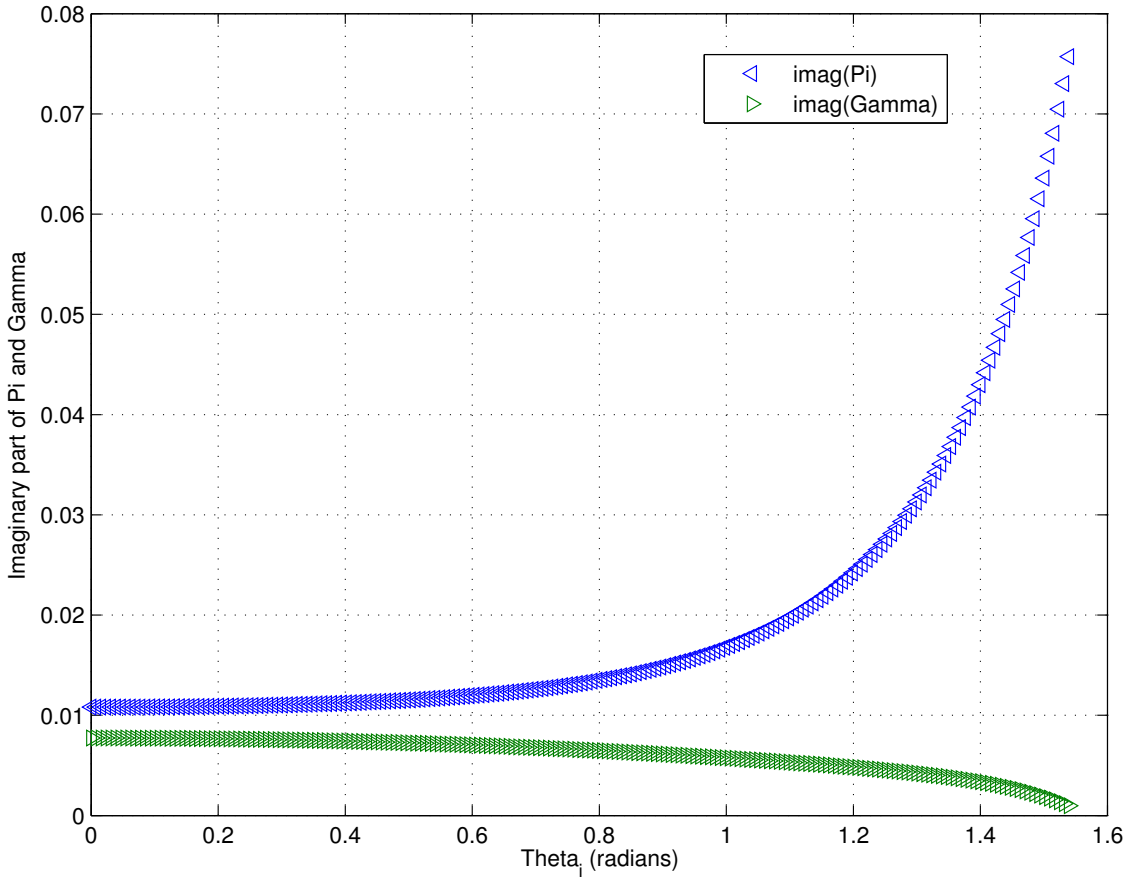

Figure 18: Verification of ILT method - imaginary part of field reflected from sand

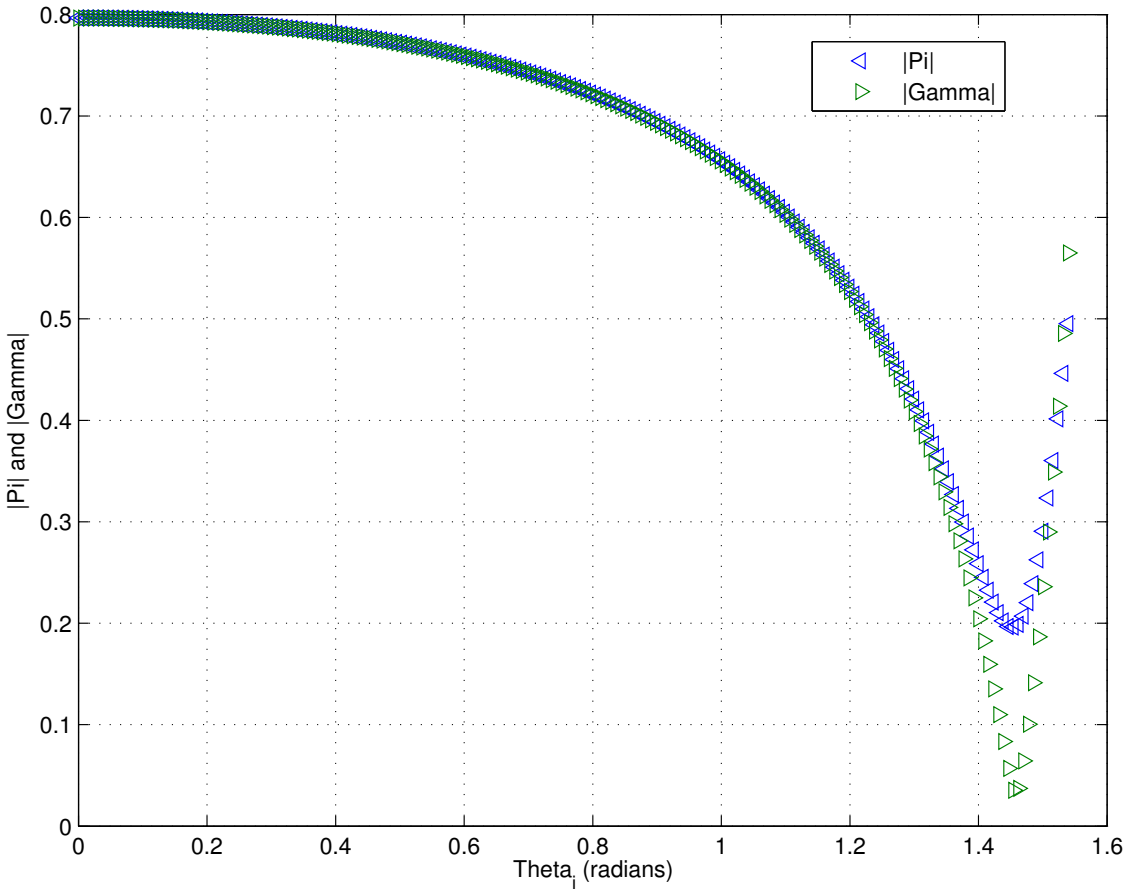

Figure 19: Verification of ILT method - magnitude of field reflected from sea water

4.2 Automated limits of integration for reflected field

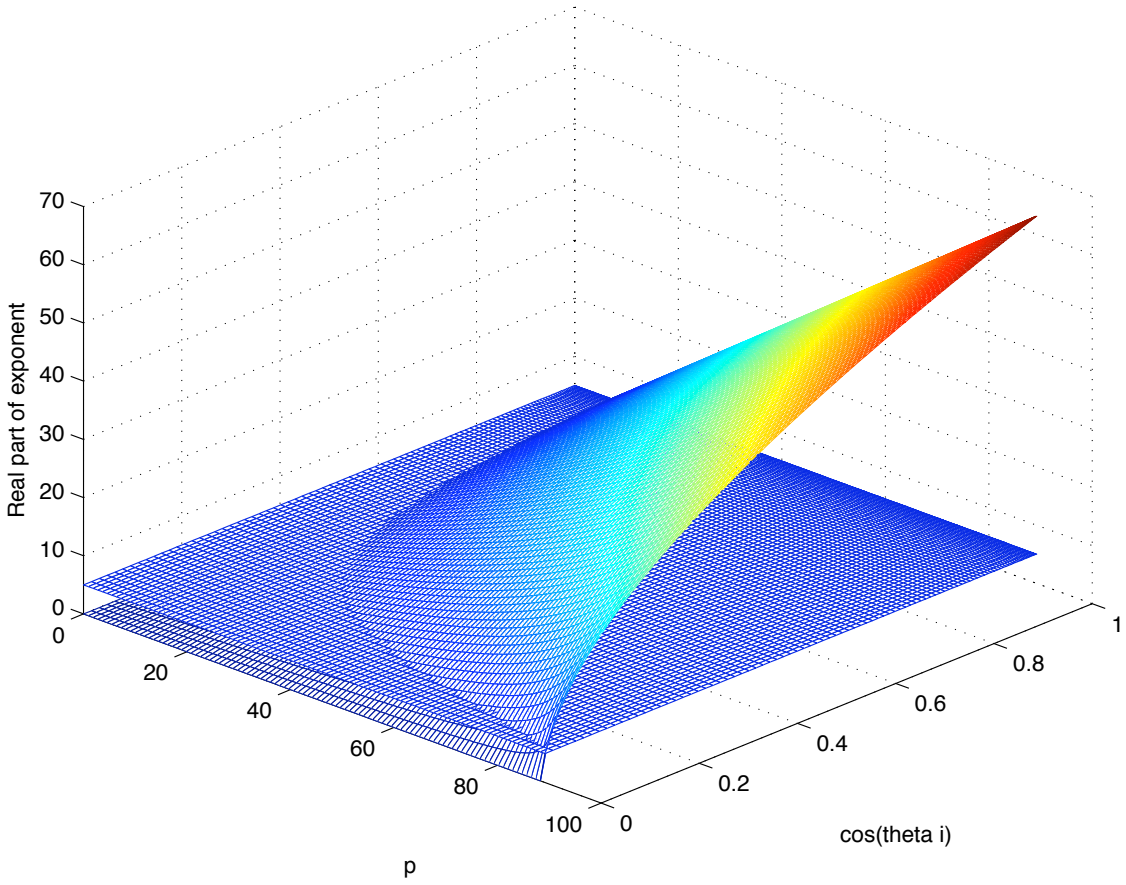

Figure 20: $\Re\{jk\zeta(\xi-1)\}$ vs p and $\cos\theta_i$

In section 4.1 we developed the following expression for the reflected potential in Eq (56):

$$\pi_r(\vec{r}) = \frac{e^{-jk\zeta}}{4\pi\zeta}\left(\frac{1-\epsilon}{1+\epsilon} + \int_0^\infty Ss(p)\frac{e^{-jk\zeta(\xi-1)}}{\xi}dp\right)$$

where, from Eq (54):

$$\xi = \sqrt{1-\left(\frac{p}{\zeta k\sqrt{\mu\epsilon-1}}\right)^2 - j\frac{2p\cos\theta_i}{\zeta k\sqrt{\mu\epsilon-1}}}$$

Obviously we can't integrate to $p = \infty$. So we need to find a function $p(\theta_i, k\zeta, \sqrt{\mu\epsilon - 1})$ that gets us "close enough". Specifically, we require that:

$$x = \Re\{jk\zeta(\xi - 1)\}, \qquad x > 5 \tag{61}$$

This situation is shown graphically in Fig 20. The plane at $z = 5$ represents the desired minimum real part of the exponent. The curved surface is $\Re\{x\}$, for the case $f = 2.4$ GHz, and $\epsilon = 3$, corresponding to a cement wall. As can be seen, $\cos\theta_i$ has a large effect on the required value of p. At $\cos(\theta_i) \approx 0$, grazing incidence, the necessary value of p is around 90. However, for normal incidence it is around 12.

To find an appropriate function of p, the intersection of the plane and surface in Fig 20, we examine two cases. In both cases, we assume that k, ζ, μ, ϵ are real, but at the end of this section we generalize to the case of lossy materials.

Case 1: $\cos\theta_i \to 0$.

In this case,

$$\xi = \sqrt{1 - \left(\frac{p}{k\zeta\sqrt{\mu\epsilon - 1}}\right)^2} \tag{62}$$

For $\Re\{x\} \neq 0$, we must have $p > k\zeta\sqrt{\mu\epsilon - 1}$. So assume this, and then we can write:

$$x = k\zeta\sqrt{\left(\frac{p}{k\zeta\sqrt{\mu\epsilon - 1}}\right)^2 - 1} \tag{63}$$

noting that in order for $x > 5$, we had to choose the negative root. Then we get:

$$p > \sqrt{(\mu\epsilon - 1)(25 + k^2\zeta^2)} \tag{64}$$

This value for p will be adequate no matter what the value of $\cos\theta_i$.

Case 2: $k\zeta\sqrt{\mu\epsilon - 1} \gg p$

In this case, the term $j\frac{-2p\cos\theta_i}{k\zeta\sqrt{\mu\epsilon - 1}}$ contributes to $\Re\{x\}$ all along. First we define:

$$w = \xi^2 = 1 - \left(\frac{p}{k\zeta\sqrt{\mu\epsilon - 1}}\right)^2 - j\frac{2p\cos\theta_i}{k\zeta\sqrt{\mu\epsilon - 1}} = a + jb \tag{65}$$

Then we can also write $w = |w|e^{j\phi}$ where $\phi = tan^{-1}\frac{b}{a}$. So:

$$\phi = tan^{-}1\left(\frac{\frac{-2p\cos\theta_i}{k\zeta\sqrt{\mu\epsilon-1}}}{1-\left(\frac{p}{k\zeta\sqrt{\mu\epsilon-1}}\right)^2}\right) \tag{66}$$

But because we assumed $k\zeta\sqrt{\mu\epsilon-1} \gg p$, we can neglect the second-order term, and take the small angle approximation, yielding:

$$\phi = \frac{-2p\cos\theta_i}{k\zeta\sqrt{\mu\epsilon-1}} \tag{67}$$

Using the same reasoning, we see that:

$$|w| = \sqrt{a^2+b^2} \approx 1 \tag{68}$$

If we express $\xi = \alpha + j\beta$ then $\Re\{x\} = -\beta k\zeta > 5$. But

$$\xi = \sqrt{w} = \sqrt{|w|}e^{j\frac{\phi}{2}} \tag{69}$$

so

$$\beta = \sin\left(\frac{-2p\cos\theta_i}{2k\zeta\sqrt{\mu\epsilon-1}}\right) \approx \frac{-p\cos\theta_i}{k\zeta\sqrt{\mu\epsilon-1}} \tag{70}$$

again by small angle approximation. Thus:

$$p > \frac{5\sqrt{\mu\epsilon-1}}{\cos\theta_i} \tag{71}$$

Though the integrands for the reflected and transmitted potential are complex, p is integrated along the real line. Our estimation of an appropriate limit of integration is based on the worst case, where ϵ and μ are purely real. If instead the material properties are complex, ξ will be complex, and thus the term $jk\zeta(\xi-1)$ will always have at least some real part. This real part helps to hasten convergence.

Therefore, we can use the following formula to find the appropriate limit of integration p when calculating the reflected field, which incorporates some margin of safety, and is valid for both dielectric and lossy media:

$$p = \min\left(\Re\left\{\frac{6\sqrt{\mu\epsilon - 1}}{\cos\theta_i}\right\}, \Re\left\{\sqrt{(\mu\epsilon - 1)(26 + k^2\zeta^2)}\right\}\right) \tag{72}$$

In the ILT-method codes, the value for p_{max} in the region of interest was found, and a lookup table for $Ss(p)$ was constructed for values of p from 0 to p_{max}. The variable `scale` determined the number of intermediate points in the table between integer values of p. When the actual integration is performed, the function `Ss_int` is called to perform linear interpolation between the closest available values for p. For most of the numerical experiments discussed in this paper, `scale` = 15.

5 Results and Discussion

In this Chapter, we first present results for the near-field and far-field reflection of 2.4 GHz radiation from a small, vertically oriented Hertzian dipole, located above a smooth plane of sand ($\epsilon = 3 - .1i$) or sea water ($\epsilon = 76 - 9i$). In all cases, the dipole was located at $z_0 = 2$ meters.

We discuss the results, including error terms in both near and far field. Then we address the issue of computer time to calculate the fields.

Finally, we conclude this work with a summary of the results, a list of open questions, and directions for future work.

5.1 Reflection from Sand, near field

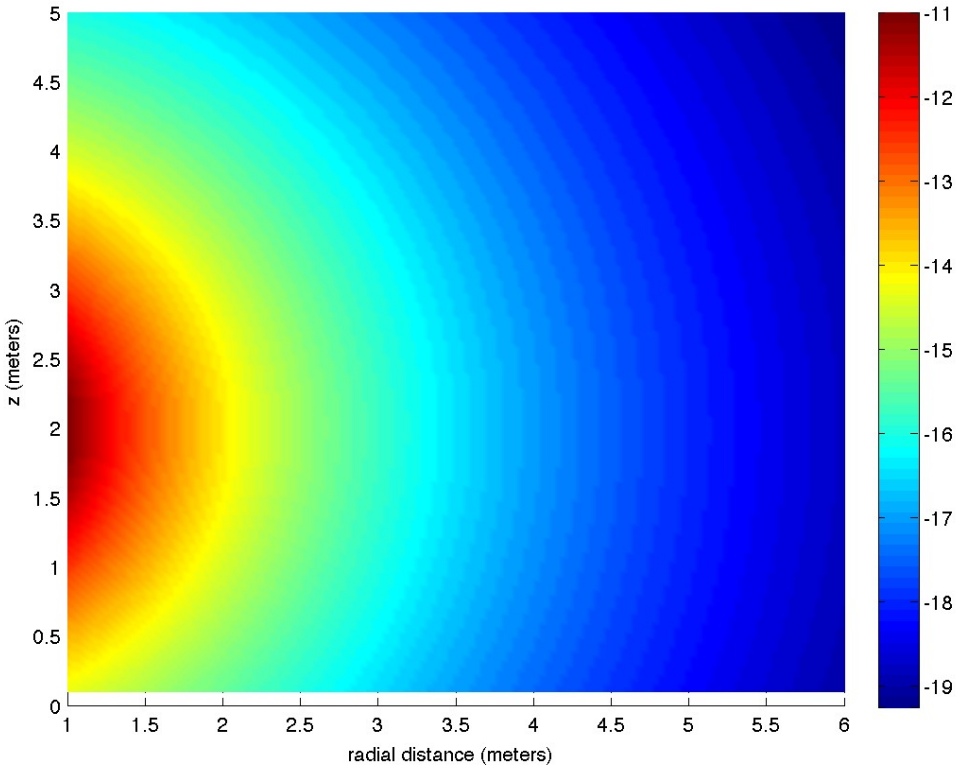

Figure 21: Incident Power, dB; Sand, near-field

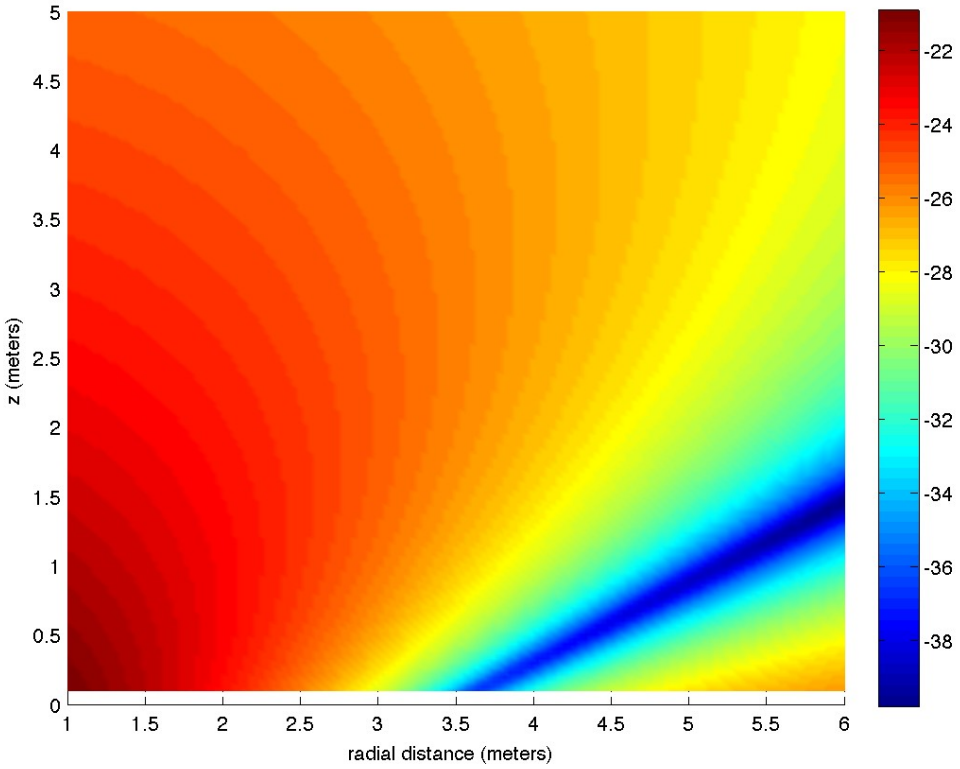

Figure 22: Reflected Power, dB; Sand, near-field

The incident near-field power from a dipole over sand is shown in Fig 21, while the reflected power is shown in Fig 22. In the plot of reflected power, the effect of the Brewster zero, corresponding to total transmission, is clearly visible as the diagonal blue region in the lower right of the figure.

The total field is shown in Fig 23, and the percentage of error in the magnitude of the power, as compared to the Sommerfeld formulation, is shown in Fig 24. The error in the near-field is less than .1% everywhere except along the exact line of the Brewster zero. Furthermore, the percentage error decreases monotonically along this line, as the distance from source to observer is increased.

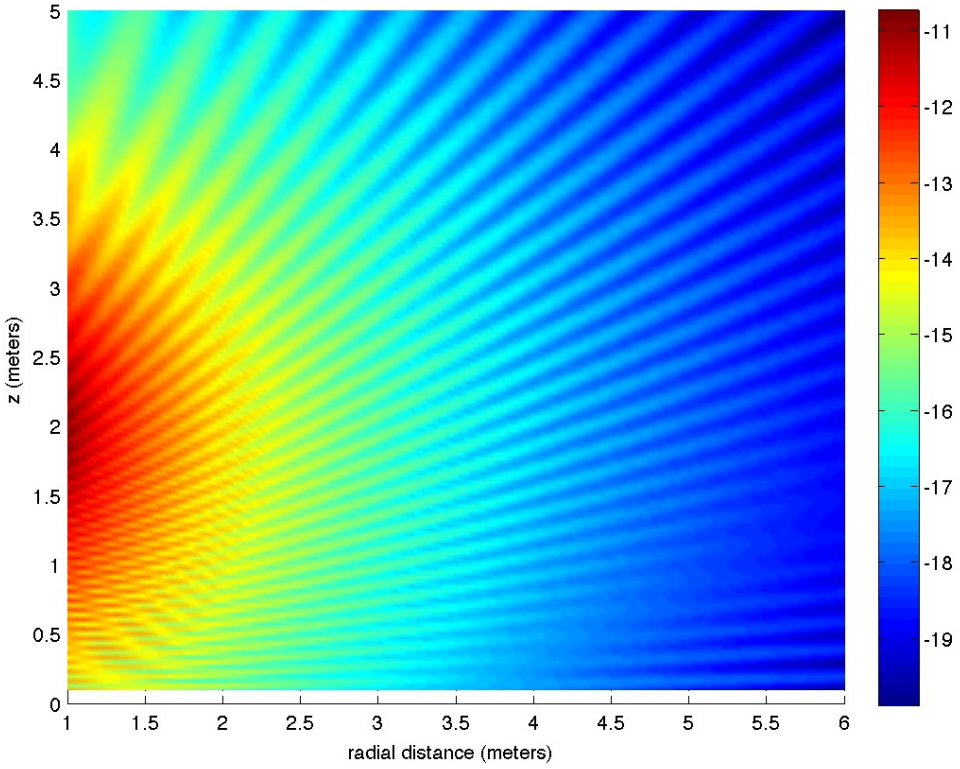

Figure 23: Total Power, dB; Sand, near-field

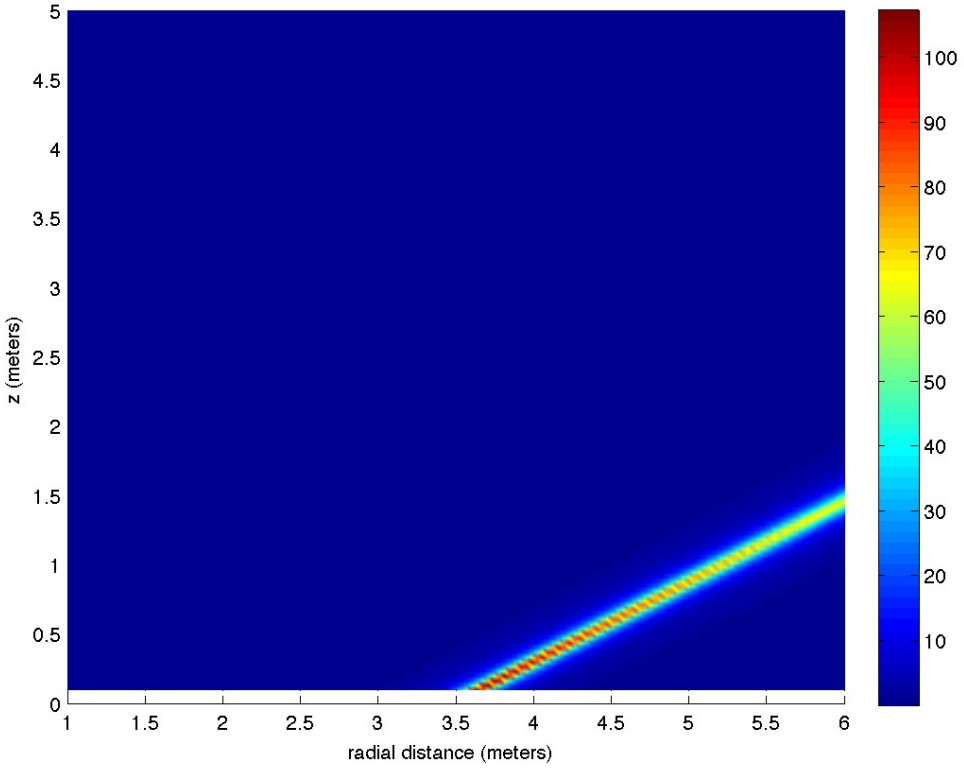

Figure 24: Percent magnitude error; Sand, near-field

5.2 Reflection from Sea Water, near field

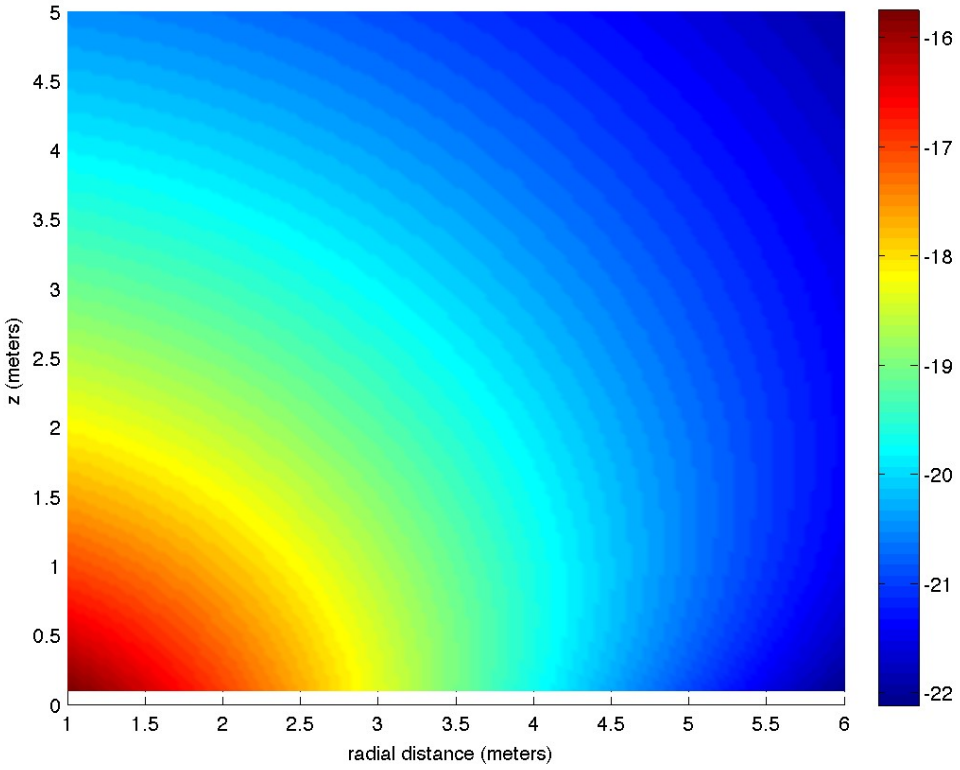

Figure 25: Reflected Power, dB; Sea, near-field

The near-field incident power above sea water is the same as in Fig 21. The reflected power is shown in Fig 25. No Brewster zero is observed in the near-field case above sea water, because the angle of the Brewster zero lies outside fo the near field. Compared to the near-field case for sand, the reflected power is more concentrated in the region below the dipole, which corresponds to normal or near-normal incidence.

The total power is shown in Fig 26, while the percentage magnitude error is shown in Fig 27. As can be seen, the error is excellent in this region, reaching a maximum of around .2% in the lower right corner.

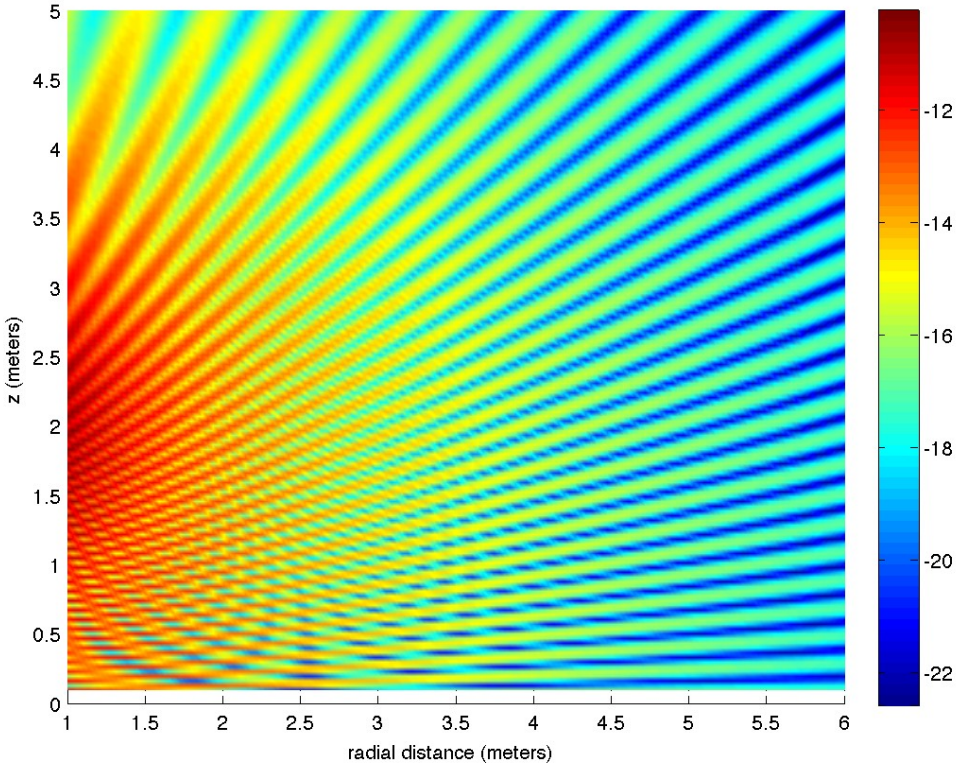

Figure 26: Total Power, dB; Sea, near-field

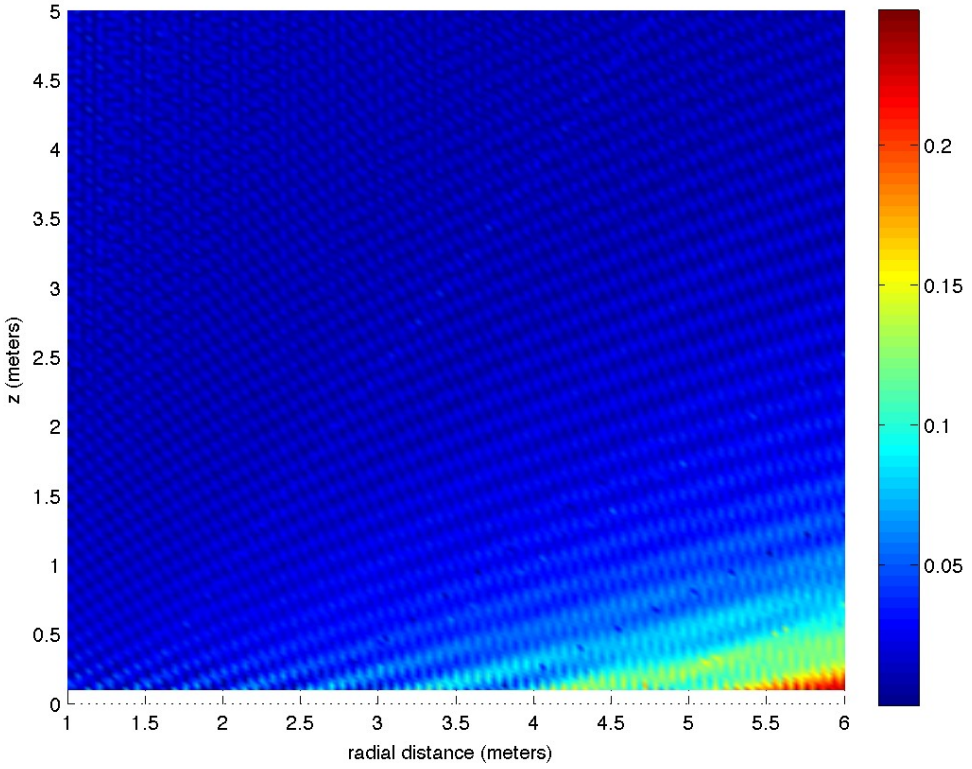

Figure 27: Percent magnitude error; Sea, near-field

5.3 Reflection from Sand, far field

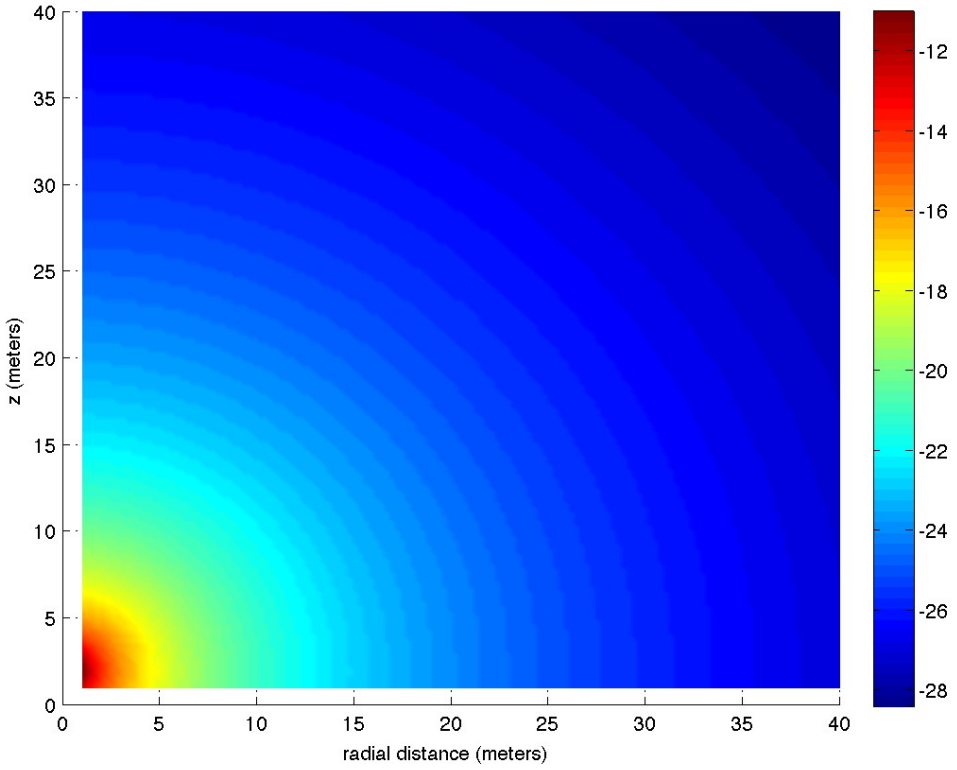

Figure 28: Incident Power, dB; Sand, far-field

The incident far-field power for the dipole over sand is shown in Fig 28. Here the effects of geometrical spreading of the power are obvious. The reflected power is shown in Fig 29. Again, the Brewster zero is clearly visible, though for angles greater than the Brewster zero, a considerable amount of power is reflected.

The total field is shown in Fig 30. The Brewster zero can still be observed, superimposed over the diffraction effects. The percentage error in power magnitude is shown in Fig 31. The percentage error is less than .1% everywhere in the far field, except for exactly along the line of the Brewster zero, where again it decreases monotonically with distance.

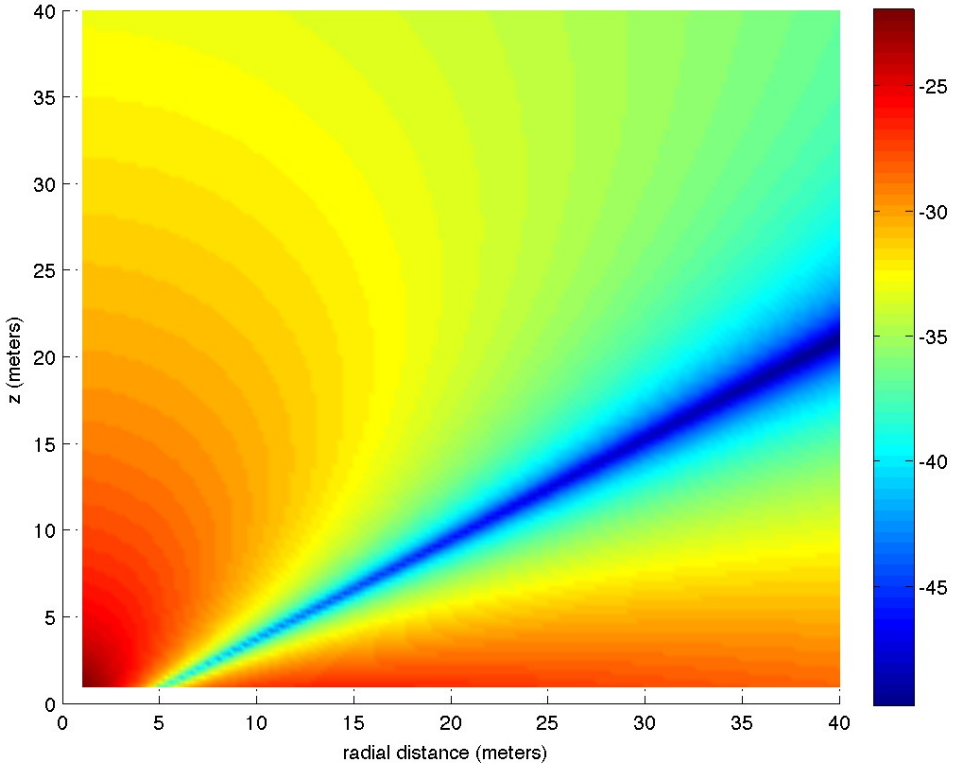

Figure 29: Reflected Power, dB; Sand, far-field

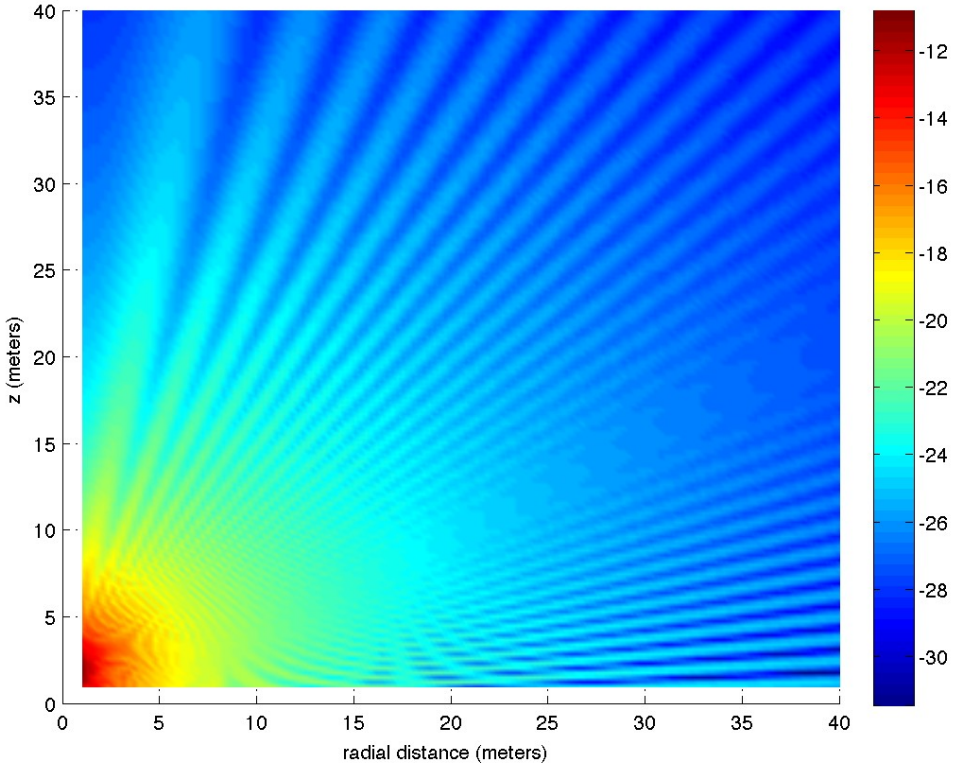

Figure 30: Total Power, dB; Sand, far-field

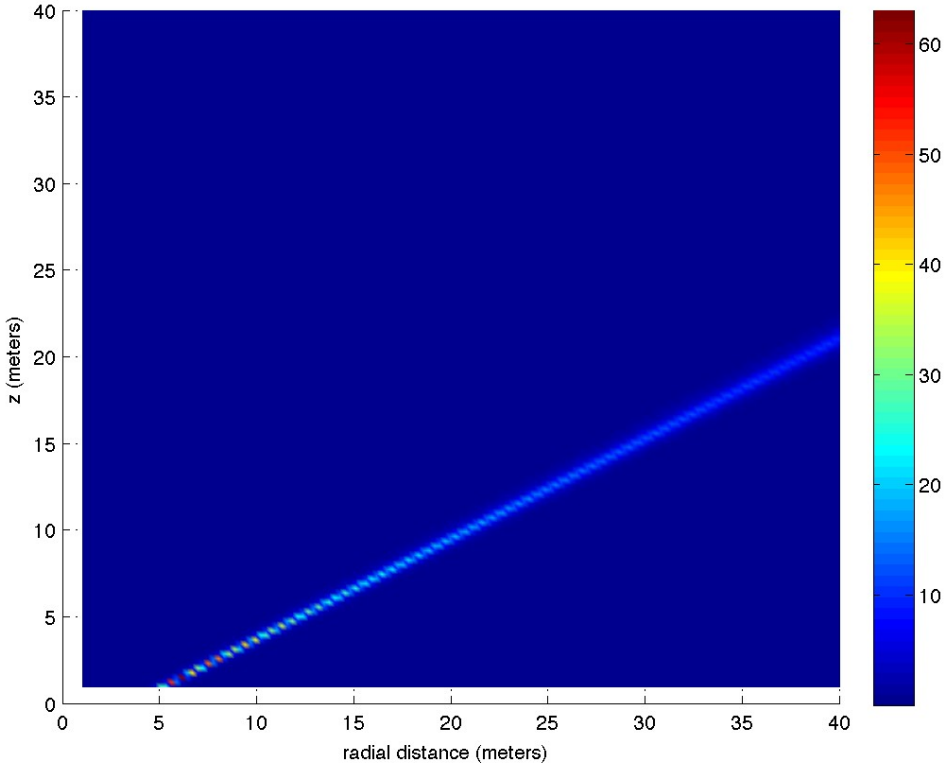

Figure 31: Percent magnitude error; Sand, far-field

5.4 Reflection from Sea Water, far field

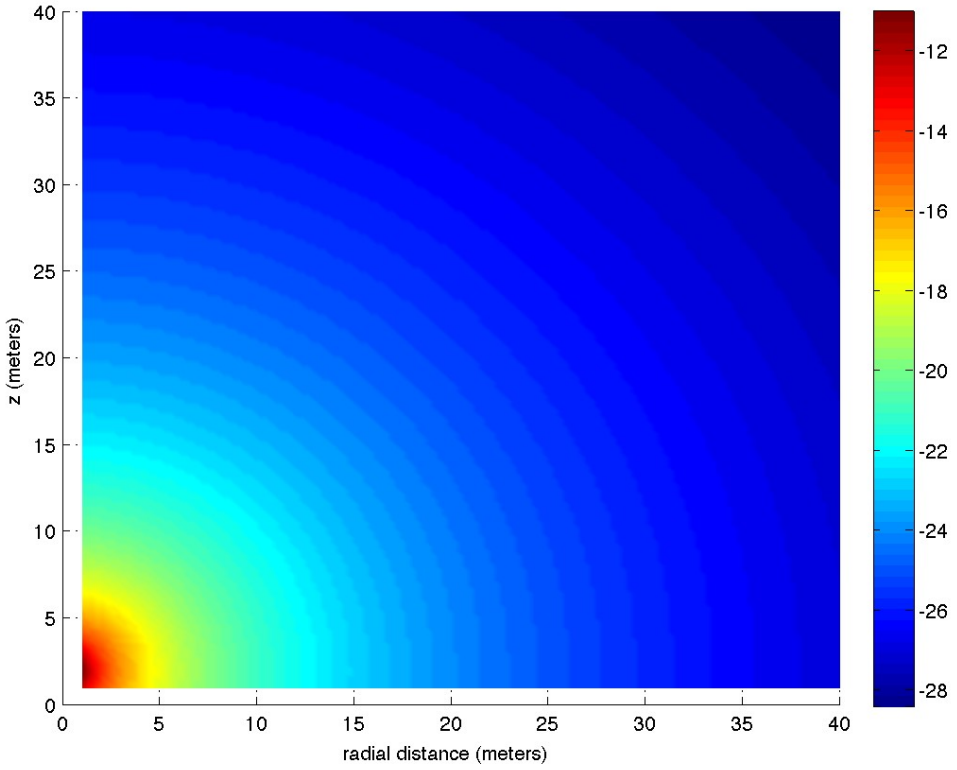

Figure 32: Incident Power, dB; Sea, far-field

The incident far-field power is the same as Fig 28, while the reflected far-field power is shown in Fig 33. For sea water, the Brewster zero lies along the material interface, as seen in the lower right corner of the plot. As opposed to the far-field reflection in sand, where there was a considerable amount of power hugging the interface at greater radial distances, here the reflected power is somewhat more constant and vertically-directed.

The total far-field power is shown in Fig 34. As in the far-field sand case, the effect of the Brewster zero is again visible, this time hugging the interface. The error plot is shown in Fig 35. The error is less than 1% everywhere in the plane, except along the Brewster zero, where it reaches a maximum of around 50%.

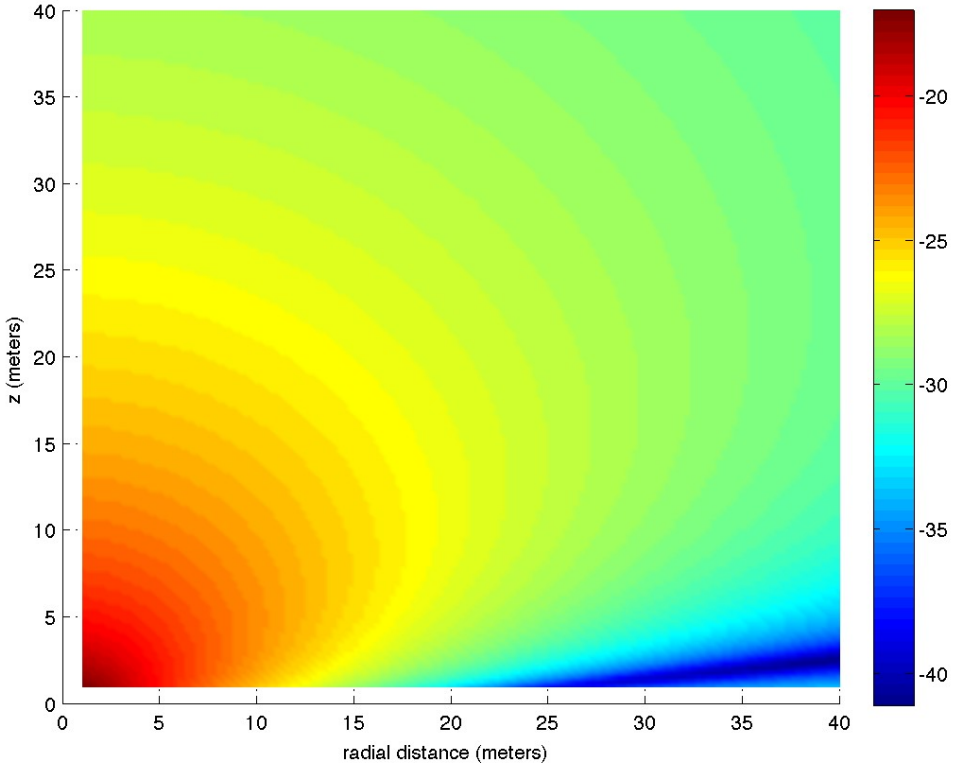

Figure 33: Reflected Power, dB; Sea, far-field

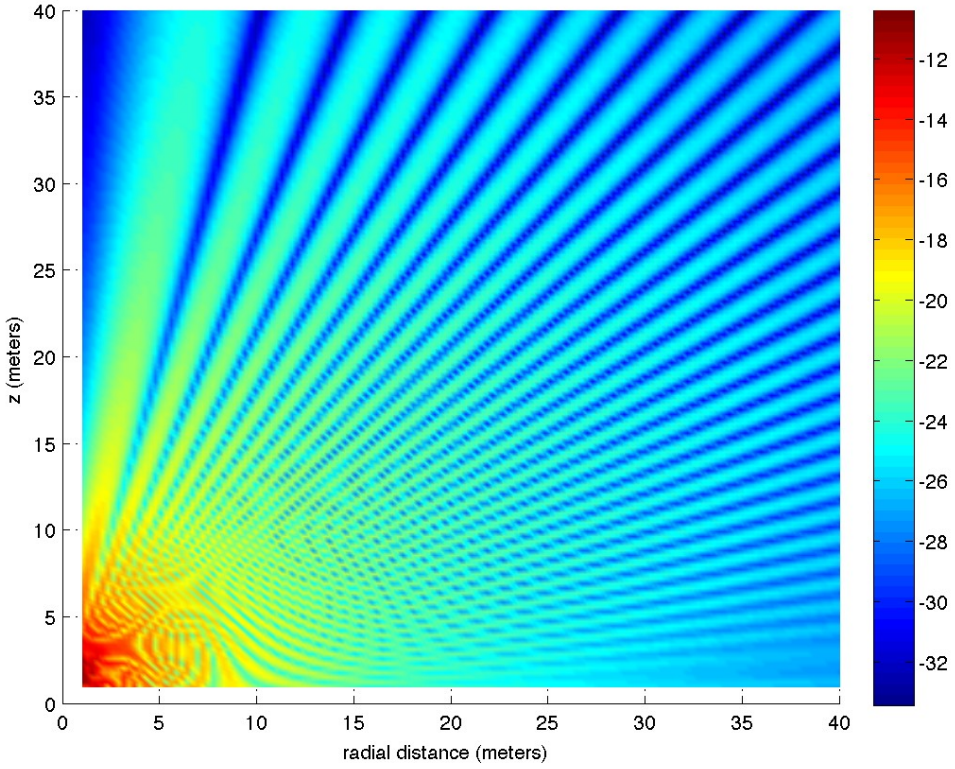

Figure 34: Total Power, dB; Sea, far-field

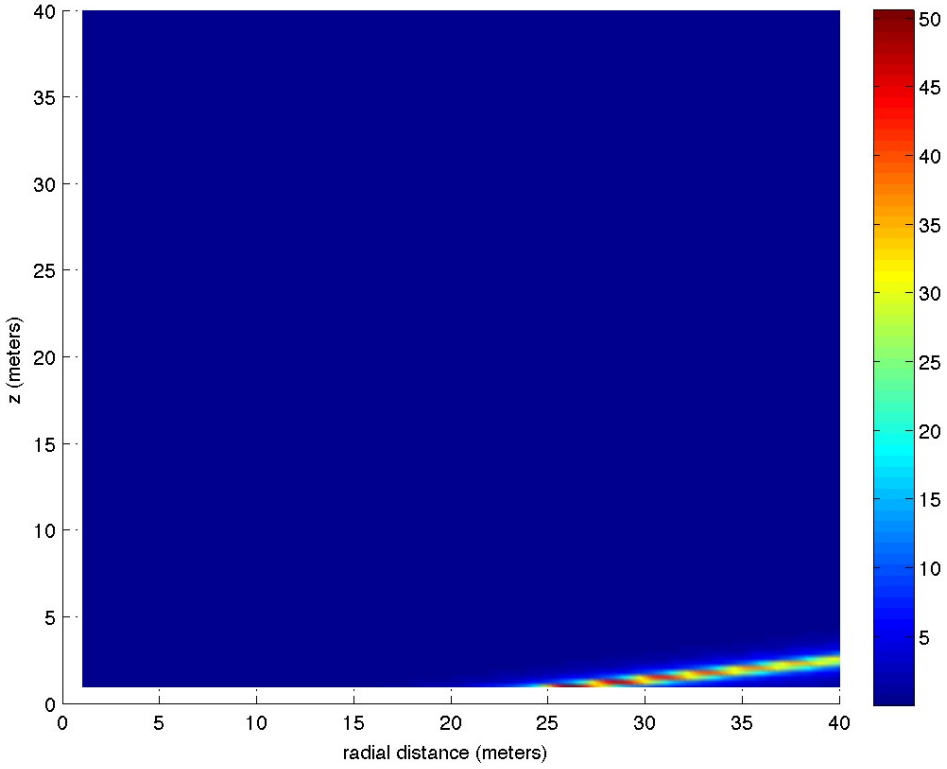

Figure 35: Percent magnitude error; Sea, far-field

5.5 ILT method around the Brewster zero

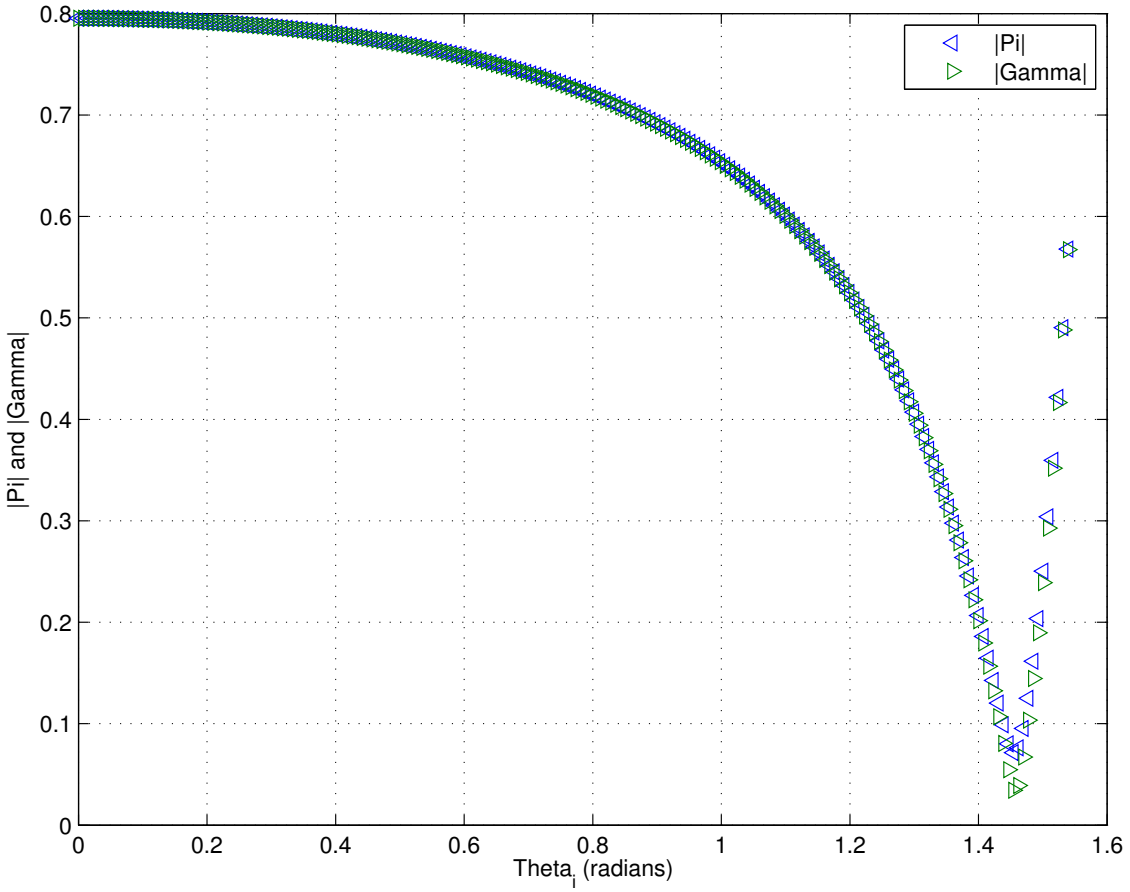

Figure 36: $\pi(\vec{r})$ vs angle, R = 10 m, sea water

As is obvious from the previous results, the ILT method offers very good accuracy, except in the vicinity of the Brewster zero. Consider again the case of a 2.4 GHz wave incident on sea water from a fixed distance as a function of angle. Referring back to Fig 19 on page 34, we saw that the agreement was acceptable, except near the Brewster zero. In that plot, the distance $R = 2$ meters, and $p_{max} = 874$. When we examine a similar scenario, but with 10 m from source to interface, the agreement is better, as shown in Fig 36. Here $p_{max} = 2763$. It is assumed that the higher value of p_{max} is assisting in achieving better agreement.

As Ishimaru notes[13] in a recent paper generalizing the half-space problem to materials of arbitrary permittivity and permeability, the Brewster Zero and Zennek pole are intimately

tied together. Using the conventions in this paper, where the magnetic component of the reflected field is assumed to be in the opposite direction from the component in the incident field, the reflection coefficient can be written as:

$$\Gamma = \frac{k_{z2}/\epsilon_2 - k_{z_1}/\epsilon_1}{k_{z2}/\epsilon_2 + k_{z_1}/\epsilon_1} \tag{73}$$

Therefore the Brewster zero is given by $k_{z_1}/\epsilon_1 = +k_{z2}/\epsilon_2$, while the Zennek pole is given by $k_{z_1}/\epsilon_1 = -k_{z2}/\epsilon_2$. Consider again the formulation for Γ in terms of the normalized variable q used in this paper, Eq (32) on page 19 (reproduced here for convenience):

$$\Gamma(q) = \frac{\sqrt{1+q^2} - \epsilon q}{\sqrt{1+q^2} + \epsilon q}$$

where $q = \cos(\theta_i)/\sqrt{\mu\epsilon - 1}$, where μ and ϵ are the normalized material properties. Then in order to find the Brewster zero q_{BZ}, we set the terms of the numerator equal to each other, square both sides, and then factor to find q. This gives us:

$$q_{BZ} = \pm\sqrt{\frac{1}{\epsilon^2 - 1}} \tag{74}$$

But following the same procedure with the denominator, in order to find the Zennek pole, we get the same result. Therefore, the issue of the Brewster Zero and Zennek pole depends intimately on the proper choice of branch cuts. The issue of branch cuts was addressed explicitly (and we believe correctly) in Section 3.3. Therefore, it will require further investigation to determine the difficulty of the ILT formulation near the Brewster Zero.

5.6 Computer Time

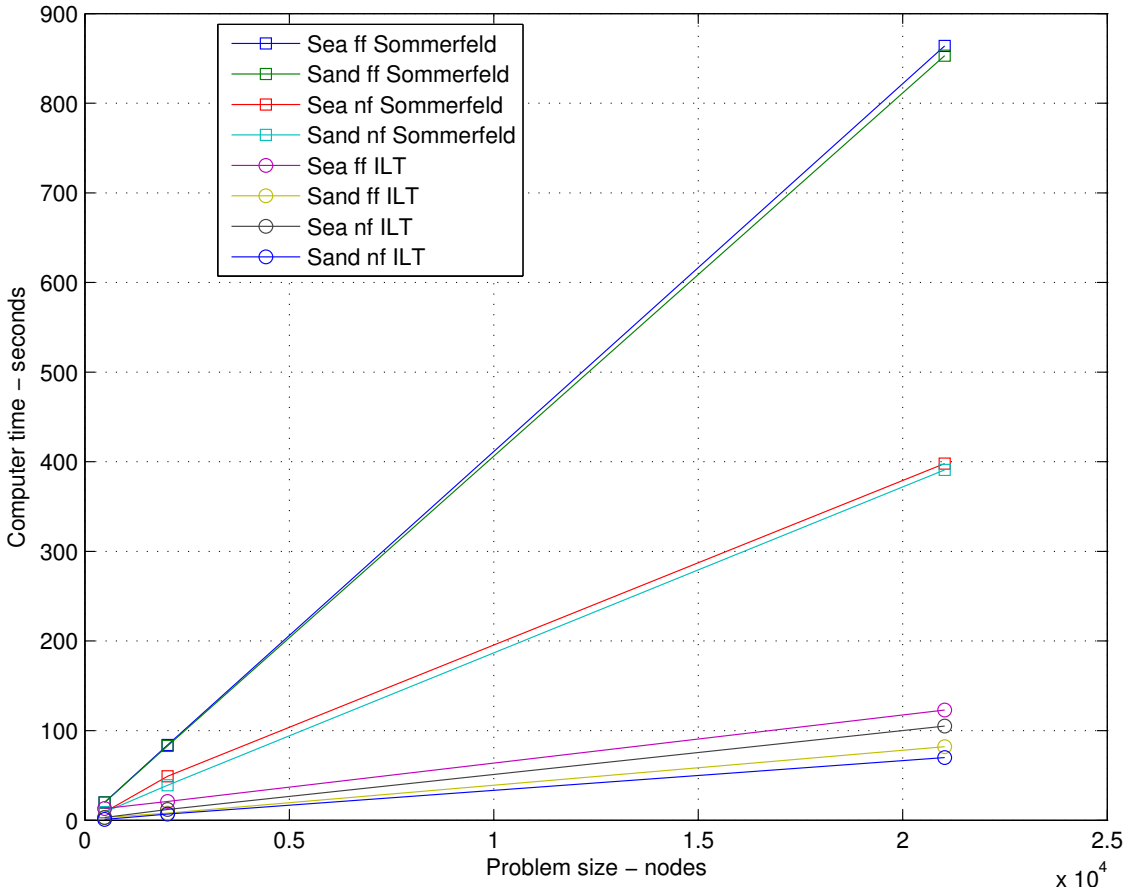

Figure 37: Problem size vs computer time

As seen in Fig 37, though both the ILT method and direct Sommerfeld evaluation scale linearly as the number of nodes calculated, the slope for the ILT method is much lower. In addition, the ILT computation times for near field and far field cases are very close, while the far field computations require significantly more time for the Sommerfeld method.

The Sommerfeld evaluation was also more prone to numerical difficulties when calculating fields far from the source. This could be mitigated by increasing the parameter ϵ (the distance by which the singularity in the integrand is avoided - see Sec 2.3, but that will also cause accuracy to suffer.

The change from near field to far field has little effect on the computer time for the ILT method, except for the overhead required to produce the lookup table for $Ss(p)$, because

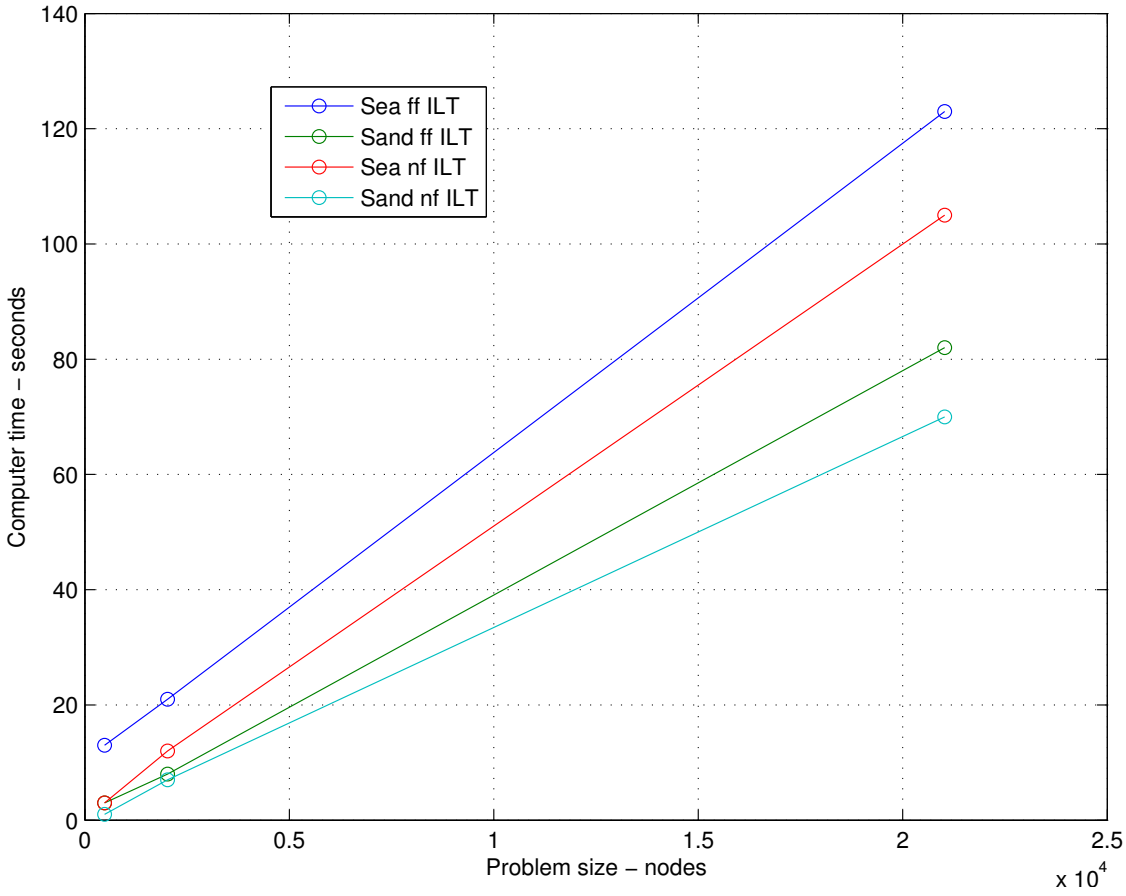

Figure 38: Problem size vs computer time – ILT solutions only

p_{max} is a function of both the material properties and the distance from the source to observer. In Fig 38 we show the computer times for the ILT method. The slopes for the two far field cases are essentially the same, but there is a time offset because p_{max} is greater for sea than for sand.

The amount of time to create the lookup table is linearly dependent on the variable `scale`, which determines the number of intermediate points between integer values of p. For all example runs in this work, `scale`= 15. However, the effect of this parameter on accuracy was not investigated in depth. If this parameter was optimized, an even greater speed increase could potentially be realized. Checking results for `scale` factors between 1 and 30 showed very little change in the calculated fields, a finding which was surprising.

5.7 Conclusion

In summary, we have described and implemented a fast method for calculating the reflected field in the presence of a conductive half-space. The method offers particular advantage for detailed calculations in the far-field region, away from the boundary, which is a challenging area for the Sommerfeld formulations.

In all cases except along the Brewster zero, the magnitude calculated by the ILT method is within 1% of that calculated by direct evaluation of the Sommerfeld integral. Furthermore, the error in magnitude is almost entirely due amplitude error in the imaginary part. Thus, if only the magnitude is needed, the ILT method should generally be acceptable.

The next steps in this research will be to generalize the method to materials of arbitrary permittivity and permeability (ie isotropic metamaterials), and to extend the method to transmission. In addition, further effort will be placed on resolving the discrepancy in the imaginary part of the field near the Brewster Zero.

6 Appendix

6.1 Notation

Electric and magnetic fields are naturally vector quantities, with magnitude and direction. Vectors will be denoted with an arrow, such as: $\vec{x}$.

The unit vectors in Cartesian coordinates will be given as: $\hat{x}, \hat{y}, \hat{z}$.

While a position is just a point, and we could notate it as (x, y, z), it will be to our benefit to use the position vector $\vec{r}$:

$$\vec{r} = \hat{x}x + \hat{y}y + \hat{z}z$$

We will also use vector functions. For example, the electric field $\vec{E}(\vec{r})$ is a function of space, which describes a field pointing somewhere else in space. We break the electric field down into its components in E_x, E_y, and E_z, and notate it as:

$$\vec{E}(\vec{r}) = \hat{x}E_x(\vec{r}) + \hat{y}E_y(\vec{r}) + \hat{z}E_z(\vec{r})$$

But sometimes, to be concise, we'll write $\vec{E_x}(\vec{r})$ or just $\vec{E_x}$ to mean $\hat{x}E_x(\vec{r})$.

We will also use scalar functions, in particular the Hertzian potential $\pi(\vec{r}, t)$, or $\pi(\vec{r}, \omega)$. Note that these are actually two different functions, one of space and time, the other of space and frequency. In ambiguous cases, clarity will be chosen over conciseness.

We will be working primarily in Cartesian coordinates, so it's safe to regard ∇ ("del") as an operator. When written next to a vector, ∇ is the gradient operator, or directional derivative. It takes a vector or scalar as input, and returns a vector as output:

$$\nabla\vec{E}(\vec{r}) = \hat{x}\frac{\partial}{\partial x}E_x(\vec{r}) + \hat{y}\frac{\partial}{\partial y}E_y(\vec{r}) + \hat{z}\frac{\partial}{\partial z}E_z(\vec{r}) \qquad \text{(gradient of vector)}$$

$$\nabla A(\vec{r}) = \hat{x}\frac{\partial}{\partial x}A(\vec{r}) + \hat{y}\frac{\partial}{\partial y}A(\vec{r}) + \hat{z}\frac{\partial}{\partial z}A(\vec{r}) \qquad \text{(gradient of scalar)}$$

Divergence is a scalar quantity. Physically, divergence can be imagined as the net flow out of or into a tiny volume. Divergence is the dot product of ∇ and a vector:

$$\nabla \cdot \vec{H}(\vec{r}, \omega) = \frac{\partial}{\partial x}H_x(\vec{r}, \omega) + \frac{\partial}{\partial y}H_y(\vec{r}, \omega) + \frac{\partial}{\partial z}H_z(\vec{r}, \omega) \qquad \text{(divergence)}$$

The curl, or circulation, of a vector, is the cross product of ∇ and the vector, usually calculated as a determinant:

$$\nabla \times \vec{D} = det \begin{vmatrix} \hat{x} & \hat{y} & \hat{z} \\ \frac{\partial}{\partial x} & \frac{\partial}{\partial y} & \frac{\partial}{\partial z} \\ D_x & D_y & D_z \end{vmatrix} \qquad \text{(curl)}$$
$$= \hat{x}(\frac{\partial}{\partial y}D_z - \frac{\partial}{\partial z}D_y) + \hat{y}(\frac{\partial}{\partial x}D_z - \frac{\partial}{\partial z}D_x) + \hat{z}(\frac{\partial}{\partial x}D_y - \frac{\partial}{\partial y}D_x)$$

Finally, we will make use of the Laplacian operator, $\nabla \cdot \nabla = \nabla^2$, as in:

$$\nabla \cdot \nabla \vec{B} = \nabla^2 \vec{B} = \frac{\partial^2}{\partial x^2}B_x + \frac{\partial^2}{\partial y^2}B_y + \frac{\partial^2}{\partial z^2}B_z$$

We will also make extensive use of complex numbers. A complex number has real and imaginary parts, for example $z = \alpha + j\beta$. The imaginary unit $j^2 = -1$. (Note that mathematics texts typically use i for the imaginary unit, while in Engineering, i is reserved for current.) Then we can write $\Re\{z\} = \alpha$ and $\Im\{z\} = \beta$ to indicate the real and imaginary parts of z, respectively.

6.2 Maxwell's Equations and the Wave Equation

All of electromagnetics is contained within Maxwell's equations, and the constitutive relations. Everything else is just elaboration. This fact is truly remarkable considering that Maxwell formulated his unified theory of electricity and magnetism before the modern era, without the benefit of any of the sophisticated test and measurement equipment we take for granted today.

Electromagnetics depends on a handful of quantities: the electric field $\vec{E}$ and flux $\vec{D}$, the magnetic field $\vec{H}$ and flux $\vec{B}$, and the material properties permittivity ϵ, permeability μ, and conductivity σ. In addition, static charge ρ, and moving charges, or current $\vec{J}$, appear. Maxwell's equations tie these parameters together in a set of four coupled partial differential equations.

The equations were initially due to Faraday, Ampère, and Gauss. Maxwell's primary contribution was to define the displacement current $\frac{\partial}{\partial t}\vec{D}$, with which he was able to formulate a unified theory of the behavior of electric and magnetic fields.

$$\nabla \times \vec{E}(\vec{r},t) = -\frac{\partial}{\partial t}\vec{B}(\vec{r},t) \qquad \text{Faraday's Law} \tag{75}$$

$$\nabla \times \vec{H}(\vec{r},t) = \frac{\partial}{\partial t}\vec{D}(\vec{r},t) + \vec{J}(\vec{r},t) \qquad \text{Maxwell-Ampère Law} \tag{76}$$

$$\nabla \cdot \vec{D}(\vec{r},t) = \rho(\vec{r},t) \qquad \text{Gauss's law} \tag{77}$$

$$\nabla \cdot \vec{B}(\vec{r},t) = 0 \qquad \text{Gauss's law for magnetism} \tag{78}$$

In addition to Maxwell's equations, we have the constitutive relationships:

$$\vec{D} = \epsilon\vec{E} \tag{79}$$

$$\vec{B} = \mu\vec{H} \tag{80}$$

$$\vec{J} = \sigma\vec{E} \tag{81}$$

In a homogenous, isotropic, time-invariant dielectic, ϵ and μ are constant, $\sigma = 0$, and therefore $\vec{J} = 0$ as well. Then we can re-write the first two of Maxwell's equations as:

$$\nabla \times \vec{E}(\vec{r},t) = -\mu\frac{\partial}{\partial t}\vec{H}(\vec{r},t) \tag{82}$$

$$\nabla \times \vec{H}(\vec{r},t) = \epsilon\frac{\partial}{\partial t}\vec{E}(\vec{r},t) \tag{83}$$

These latter formulations are particularly useful. In fact, we will now use Eq (82) and Eq (83) to derive the wave equation. To start, we take the curl of both sides of Eq (82):

$$\begin{aligned}\nabla \times (\nabla \times \vec{E}(\vec{r},t)) &= \nabla \times (-\mu\frac{\partial}{\partial t}\vec{H}(\vec{r},t)) \\ &= -\mu\frac{\partial}{\partial t}(\nabla \times \vec{H}(\vec{r},t)) \\ &= -\mu\epsilon\frac{\partial^2}{\partial t^2}\vec{E}(\vec{r},t)\end{aligned} \tag{84}$$

To finish decoupling the equations, we make use of the vector identity

$$\nabla \times \nabla \times \vec{E} = \nabla(\nabla \cdot \vec{E}) - \nabla^2\vec{E}$$

and the fact that

$$\nabla \cdot \vec{E}(\vec{r},t) = \frac{1}{\epsilon}\rho(\vec{r},t)$$

to obtain:

$$\nabla^2 \vec{E}(\vec{r},t) - \mu\epsilon\frac{\partial^2}{\partial t^2}\vec{E}(\vec{r},t) = \frac{1}{\epsilon}\nabla\rho(\vec{r},t) \tag{85}$$

In a source free region, ie with no charges around, this reduces to the familiar free-space wave equation:

$$\nabla^2 \vec{E}(\vec{r},t) - \mu\epsilon\frac{\partial^2}{\partial t^2}\vec{E}(\vec{r},t) = 0 \tag{86}$$

6.3 The Fourier Transform and the Dispersion Relation

Anyone who has studied electromagnetics has certainly encountered a wavenumber, usually denoted k. But where does this wavenumber actually come from? The units of k are $\frac{rad}{m}$, which gives us a clue.

The Fourier Transform (FT) is most well-known as a method to break a complex periodic signal into sinusoid components of different frequencies. Another way to put it is that the FT is a bridge between the time and frequency domains.

Given a time-domain signal $f(t)$, by definition its FT $F(\omega)$ is given by:

$$F(\omega) = \int_{-\infty}^{+\infty} f(t)e^{-j\omega t}dt \tag{87}$$

To obtain $f(t)$ from $F(\omega)$, we use the Inverse Fourier Transform (IFT):

$$f(t) = \frac{1}{2\pi}\int_{-\infty}^{+\infty} F(\omega)e^{j\omega t}d\omega \tag{88}$$

Note however that there is nothing sacred about time and frequency in the FT and IFT; rather, it is the form that is important. For example, consider the amplitude of a standing wave given by $f(z) = A_0 \cos kz$. Then we find $F(k)$ as:

$$F(k) = \int_{-\infty}^{+\infty} f(z) e^{-jkz} dz$$

Here $F(k)$ gives us the amplitude of the wave as a function of wavenumber. In the time-frequency case, ω has units $\frac{rad}{s}$, while time is in s. In the space-wavenumber case, k has units $\frac{rad}{m}$, while space is in m. One could say that ω measures the distance in time between wave fronts, while k measures the distance in space between wave fronts.

Electromagnetics relies on the idea of inverse physical-space FT's. Frequently, we'll want to go a step further, and represent a time- and space-dependent field as the IFT of a four-dimensional FT:

$$\vec{E}(\vec{r}, t) = \left(\frac{1}{2\pi}\right)^4 \iiiint \vec{E}(\vec{k}, \omega) e^{j(\omega t - \vec{k}\cdot\vec{r})} d\vec{k} d\omega \tag{89}$$

where the limits of all four integrals are $-\infty$ to $+\infty$, $\vec{k} \cdot \vec{r} = xk_x + yk_y + zk_z$, and $d\vec{k}$ is shorthand for $dk_x dk_y dk_z$. Notice that we're using the $e^{j\omega t}$ convention. Thus, e^{-jzk_z} corresponds to propagation wave in the $+z$ direction.

If our medium is homogeneous, isotropic, and time-invariant, then we can pull operators such as ∇^2 and $\frac{\partial}{\partial t}$ inside the integrals. After all, ∇^2 only operates on the $e^{-j\vec{k}\cdot\vec{r}}$ factor, and $\frac{\partial}{\partial t}$ only operates on the $e^{j\omega t}$ factor.

Now we can reconsider our wave equation (86), using the four dimensional space-time FT of $\vec{E}(\vec{r}, t)$ (89). Let's examine the leftmost term of Eq (86) first.

$$\begin{aligned}
\nabla^2 \left(\frac{1}{2\pi}\right)^4 \iiiint \vec{E} e^{j\omega t} e^{-j\vec{k}\cdot\vec{r}} d\vec{k} d\omega &= \left(\frac{1}{2\pi}\right)^4 \iiiint \vec{E} e^{j\omega t} \nabla^2 e^{-j\vec{k}\cdot\vec{r}} d\vec{k} d\omega \\
&= \left(\frac{1}{2\pi}\right)^4 \iiiint \vec{E} e^{j\omega t} (-k_x^2 - k_y^2 - k_z^2) e^{-j\vec{k}\cdot\vec{r}} d\vec{k} d\omega
\end{aligned}$$

As for the second term on the left hand side of Eq (86):

$$\begin{aligned}
-\frac{\partial^2}{\partial t^2} \mu\epsilon \left(\frac{1}{2\pi}\right)^4 \iiiint \vec{E} e^{j\omega t} e^{-j\vec{k}\cdot\vec{r}} d\vec{k} d\omega &= -\mu\epsilon \left(\frac{1}{2\pi}\right)^4 \iiiint \vec{E} \frac{\partial^2}{\partial t^2} e^{j\omega t} e^{-j\vec{k}\cdot\vec{r}} d\vec{k} d\omega \\
&= +\omega^2 \mu\epsilon \left(\frac{1}{2\pi}\right)^4 \iiiint \vec{E} e^{j\omega t} e^{-j\vec{k}\cdot\vec{r}} d\vec{k} d\omega
\end{aligned}$$

Putting these results together and combining the integrals, we get:

$$\left(\frac{1}{2\pi}\right)^4 \iiint\!\!\iint \vec{E}(\vec{k},\omega)e^{j\omega t}e^{-j\vec{k}\cdot\vec{r}}(-k_x^2-k_y^2-k_z^2+\omega^2\mu\epsilon)d\vec{k}d\omega = 0$$

In order for this to be true for all space and time, we set $(-k_x^2-k_y^2-k_z^2+\omega^2\mu\epsilon)=0$. Remember that $\vec{k}=\hat{x}k_x+\hat{y}k_y+\hat{z}k_z$, or $k^2=k_x^2+k_y^2+k_z^2$. Therefore:

$$k^2=\omega^2\mu\epsilon \tag{90}$$

This important result is known as the dispersion relation. It relates the magnitude of the wavenumber vector k to the frequency of the wave ω and the material properties μ and ϵ.

Now we can revisit the wave equation which we derived in section 6.2. In a dielectric, $\sigma=0$. But for a lossy medium, $\sigma\neq 0$. So returning to Eq (84), now we include the effect of $\sigma>0$:

$$\nabla\times(\nabla\times\vec{E}(\vec{r},t)) = -\mu\epsilon\frac{\partial^2}{\partial t^2}\vec{E}(\vec{r},t)-\sigma\frac{\partial}{\partial t}\vec{E}(\vec{r},t) \tag{91}$$

If we now replace $\vec{E}(\vec{r},t)$ by $\vec{E}(\vec{r},\omega)e^{j\omega t}$, we can take the time derivatives, and write:

$$\nabla\times(\nabla\times\vec{E}(\vec{r},\omega)e^{j\omega t}) = \left(\omega^2\mu\epsilon\vec{E}(\vec{r},\omega)-j\omega\sigma\vec{E}(\vec{r},\omega)\right)e^{j\omega t} \tag{92}$$

Using the $\nabla\times(\nabla\times\vec{E})$ vector identity from section 6.2, we can write:

$$\nabla^2\vec{E}(\vec{r},\omega)+\omega^2\mu\epsilon_c\vec{E}(\vec{r},\omega)=\nabla\left(\frac{\rho}{\epsilon}\right) \tag{93}$$

where we define the complex permittivity $\epsilon_c=\epsilon(1-j\frac{\sigma}{\epsilon\omega})$. In lossy and conductive media, ϵ is in general complex. In most of the formulas we use, we can use ϵ_c where ϵ is notated. However, this is not always the case, as Eq (93) shows. In the term $\frac{\rho}{\epsilon}$ we need to use ϵ, the real part of the permittivity.

When considering wave propagation, $\Re\{\epsilon_c\}$ relates to the wavenumber, while $\Im\{\epsilon_c\}$ relates to attenuation of the wave. Essentially, a part of the energy carried by the wave turns into a current in the conducting medium, leaving the wave. Therefore, for the convention $e^{j\omega t-\vec{k}\cdot\vec{r}}$, where for example e^{-jzk_z} represents propagation in the $+z$ direction, $\Im\{\epsilon_c\}<0$. Otherwise the amplitude of the wave grows exponentially as the wave propagates. While

in fact this is true in certain physical situations, like lasers, the passive medium convention is that waves attenuate while propagating through non-dielectric media. Or in the words of J.R. Wait, we should "reject infinite physical quantities."[11]

6.4 Laplace Transform

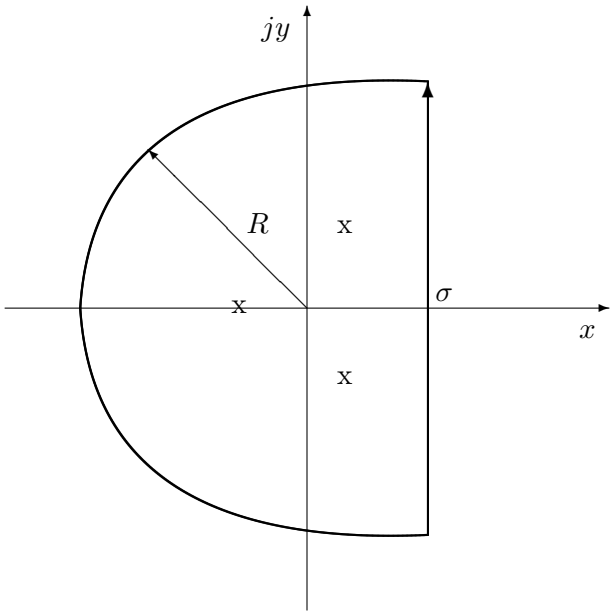

Figure 39: Closing the contour in the complex plane

The Laplace Transform (LT) can be thought of as a generalization of the Fourier Transform. The FT is calculated as a line integral along the Imaginary axis, whereas the LT includes sections of the complex plane. The FT only gives information about steady-state behavior, while the LT gives additional information about growth and decay over time.

For the frequency-domain transform, the FT variable, ω, is only evaluated along the imaginary axis. But the LT variable, $s = \sigma + j\omega$, has both real and imaginary parts. This variable sits in an exponential $e^{\pm st}$. Therefore the imaginary part ω corresponds to frequency, but the real part corresponds to exponential growth or decay.

By definition, the LT of $f(t)$ is:

$$F(s) = \int_{-\infty}^{\infty} f(t)e^{-st}dt \tag{94}$$

There is some subtlety in the LT, because the integral will only converge for certain values of s. Thus, in formal analytical work, LT's are often specified along with their region of convergence.

The Inverse Laplace Transform (ILT) of $F(s)$ is defined as:

$$f(t) = \frac{1}{j2\pi} \int_{\sigma-j\infty}^{\sigma+j\infty} F(s)e^{st}ds \tag{95}$$

There is also subtlety in the evaluation of the ILT, because in general the line integral is impossible to evaluate on its own. We choose $\sigma = \Re\{s\}$ to be to the right of all poles, though its specific value is not important. Then, we connect the ends of the line integral with a contour, as shown in Fig 39. Now because all the poles are enclosed within a simply close curve, we can invoke Cauchy's Integral Formula. In order to do this, the value of the integrand needs to go to 0 as the radius of the contour goes to infinity. So the integrand must be a proper, rational fraction.

6.5 Hankel Transform

The Hankel Transform is outlined in the Bateman *Tables of Integral Transforms*[15]. From Vol II, page 7, Hankel Transform #5:

$$\int_0^{k-} \frac{\sqrt{\rho}}{\sqrt{k^2-\rho^2}} J_0(\gamma\rho)\sqrt{\gamma\rho}d\rho = \frac{\sin(k\gamma)}{\sqrt{\gamma}} \tag{96}$$

where $k-$ is taken as infinitesimally less than k. From the same page, Transform #6:

$$\int_{k+}^{\infty} \frac{\sqrt{\rho}}{\sqrt{\rho^2-k^2}} J_0(\gamma\rho)\sqrt{\gamma\rho}d\rho = \frac{\cos(k\gamma)}{\sqrt{\gamma}} \tag{97}$$

where $k+$ is infinitesimally greater than k.

From Vol II, page 40, Hankel Transform #48:

$$\frac{1}{\sqrt{y}} \int_0^{\infty} \frac{cos(b\sqrt{a^2-x^2})}{\sqrt{a^2-x^2}} J_0(xy)x\sqrt{y}\,dx = \sqrt{\frac{\pi a}{2\sqrt{a^2-x^2}}} J_{\frac{1}{2}}(a\sqrt{b^2+y^2}) \tag{98}$$

The corresponding form for the sin function is HT #23, page 35:

$$\frac{1}{\sqrt{y}}\int_0^\infty \frac{sin(b\sqrt{a^2-x^2})}{\sqrt{a^2-x^2}}J_0(xy)x\sqrt{y}\,dx = \sqrt{\frac{\pi a}{2\sqrt{a^2-x^2}}}Y_{\frac{1}{2}}(a\sqrt{b^2+y^2}) \tag{99}$$

These transforms can be further simplified with the use of spherical Bessel functions, as outlined in Ambramowitz and Stegun[16] pages 437-438:

$$\sqrt{\frac{\pi}{2z}}J_{\frac{1}{2}}(z) = j_0(z) = \frac{sin(z)}{z} \tag{100}$$

and:

$$\sqrt{\frac{\pi}{2z}}Y_{\frac{1}{2}}(z) = y_0(z) = \frac{-cos(z)}{z} \tag{101}$$

Using both identities together, and noting that the $\sqrt{y}$ term cancels, we get:

$$\int_0^\infty \frac{cos(b\sqrt{a^2-x^2})}{\sqrt{a^2-x^2}}J_0(xy)x\,dx = \frac{sin(a\sqrt{b^2+y^2})}{a\sqrt{b^2+y^2}} \tag{102}$$

$$\int_0^\infty \frac{sin(b\sqrt{a^2-x^2})}{\sqrt{a^2-x^2}}J_0(xy)x\,dx = -\frac{cos(a\sqrt{b^2+y^2})}{a\sqrt{b^2+y^2}} \tag{103}$$

References

[1] A. Sommerfeld, *Propagation of Waves in Wireless Telegraphy*, Ann. Phys. (Leipzig), **28**, 1909, pp. 665-737.

[2] A. Sommerfeld, *Propagation of Waves in Wireless Telegraphy*, Ann. Phys. (Leipzig), **81**, 1926, pp. 1135-1153.

[3] J.R. Wait, *The Ancient and Modern History of EM Ground Wave Propagation*, IEEE Anennas and Propagation Magazine, Vol. 40, No. 5, October 1998, pp. 7-24.

[4] R.E. Collin, *Hertzian Dipole Radiating over a Lossy Earth or Sea: Some Early and Late 20^{th} Century Controversies*, IEEE Anennas and Propagation Magazine, Vol. 46, No. 2, April 2004, pp. 64-79.

[5] A. Baños *Dipole Radiation in the Presence of a Conducting Halfspace*. New York: Pergamon Press, 1966.

[6] I. Lindell and E. Alanen, *Exact Image Theory for the Sommerfeld Half-Space Problem, Part I: Vertical Magnetic Dipole*, IEEE Trans. Antennas and Prop., **AP-32**,1984, pp. 126-133.

[7] I. Lindell and E. Alanen, *Exact Image Theory for the Sommerfeld Half-Space Problem, Part II: Vertical Electric Dipole*, IEEE Trans. Antennas and Prop., **AP-32**,1984, pp. 841-847.

[8] I. Lindell and E. Alanen, *Exact Image Theory for the Sommerfeld Half-Space Problem, Part III: General Formulation*, IEEE Trans. Antennas and Prop., **AP-32**,1984, pp. 1027-1032.

[9] M. Raspopovic, *Exact Image Theory for Ultra-Wideband Pulse Reflections*, MSEE Thesis, Department of ECE, University of Massachusetts, Lowell, 2003.

[10] A. Sommerfeld, E.G. Strauss (translator) *Partial Differential Equations in Physics*. New York: The Academic Press, 1949.

[11] J.R. Wait, *Electromagnetic Wave Theory*. New York: Harper and Row, 1985.

[12] A. Ishimaru, *Electromagnetic Waves Propagation, Radiation, and Scattering*. Englewood Cliffs, NJ: Prentice Hall, 1991.

[13] A. Ishimaru, J.R. Thomas, and S. Jaruwatanadilok, *Electromagnetic Waves Over Half-Space Metamaterials of Arbitrary Permittivity and Permeability*, IEEE Trans. Antennas and Prop., **53**, 2005, pp. 915-921. (1957), 417–434.

[14] J.R. Wait, *Image Theory of a Quasistatic Magnetic Dipole over a Dissipative Half-Space*, Electron. Let., **5** no. 13, 1969, pp. 281-282.

[15] A. Erdelyi, editor, *Tables of Integral Transforms*. New York: McGraw Hill, 1954.

[16] M. Abramowitz and I. A. Stegun, *Handbook of Mathematical Functions*. New York: Dover, 1965.